Journal of Petrology Advance Access published June 13, 2005

Wolf Volcano, Galápagos Archipelago: Melting and Magmatic Evolution at the Margins of a Mantle Plume

DENNIS J. GEIST[1]*, TERRY R. NAUMANN[2], JARED J. STANDISH[3], MARK D. KURZ[4], KAREN S. HARPP[5], WILLIAM M. WHITE[6] AND DANIEL J. FORNARI[3]

[1]DEPARTMENT OF GEOLOGICAL SCIENCES, UNIVERSITY OF IDAHO-3022, MOSCOW, ID 83844, USA

[2]DEPARTMENT OF GEOLOGY, UNIVERSITY OF ALASKA ANCHORAGE, ANCHORAGE, AK 99508, USA

[3]DEPARTMENT OF GEOLOGY AND GEOPHYSICS, MASSACHUSETTS INSTITUTE OF TECHNOLOGY/WOODS HOLE OCEANOGRAPHIC INSTITUTION JOINT PROGRAM, WOODS HOLE, MA 02543, USA

[4]DEPARTMENT OF MARINE CHEMISTRY AND GEOCHEMISTRY, WOODS HOLE OCEANOGRAPHIC INSTITUTION, WOODS HOLE, MA 02543, USA

[5]DEPARTMENT OF GEOLOGY, COLGATE UNIVERSITY, HAMILTON, NY 13323, USA

[6]DEPARTMENT OF GEOLOGICAL SCIENCES, CORNELL UNIVERSITY, ITHACA, NY 14853, USA

RECEIVED JUNE 10, 2004; ACCEPTED APRIL 11, 2005

Wolf volcano, an active shield volcano on northern Isabela Island in the Galápagos Archipelago, has undergone two major stages of caldera collapse, with a phase of partial caldera refilling between. Wolf is a typical Galápagos shield volcano, with circumferential vents on the steep upper carapace and radial vents distributed in diffuse rift zones on the shallower-sloping lower flanks. The radial fissures continue into the submarine environment, where they form more tightly focused rift zones. Wolf's magmas are strikingly monotonous: estimated eruptive temperatures of the majority of lavas span a total of only 22°C. This homogeneity is attributed to buffering of magmas as they ascend through a thick column of olivine gabbroic mush that has been deposited from a thin, shallow (<2 km deep) subcaldera sill that is in a thermochemical steady state. Wolf's lavas have the most depleted isotopic compositions of any historically active intraplate ocean island volcano on the planet and have isotopic compositions (except for $^3He/^4He$) indistinguishable from mid-ocean ridge basalt erupted from the Galápagos Spreading Center (GSC) 250–410 km away from the peak of influence of the Galápagos plume. Wolf's lavas are enriched in incompatible trace elements and have systematic major element differences relative to GSC lavas, however. Wolf's magmas result from lower extents of melting, deeper melt extraction, and a greater influence of garnet compared with GSC magmas, but Wolf and the GSC share the same sources. These melt generation conditions are attributed to melting in a thermal and mechanical boundary layer of depleted asthenosphere at the margins of the Galápagos plume. The lower degrees of melting and extraction from deeper levels result from a thicker lithospheric cap at Wolf than exists at the GSC.

KEY WORDS: *caldera; Galápagos; mush; partial melting; plume*

INTRODUCTION

Wolf volcano forms the northeastern part of Isabela Island in the western Galápagos Archipelago (Fig. 1) and is a geomorphological archetype of a Galápagos shield volcano (Williams & McBirney, 1979). It is the tallest Galápagos volcano (1710 m) and has undergone cyclic filling and collapse of its caldera, providing an opportunity to assess the lithospheric evolution of Galápagos magmas under changing conditions. Despite the similarity of its volcanic features and the lithospheric evolution of its magmas, Wolf volcano differs from the other western Galápagos shields in that its lavas have

*Corresponding author. Telephone: 208-885-6491. E-mail: dgeist@uidaho.edu

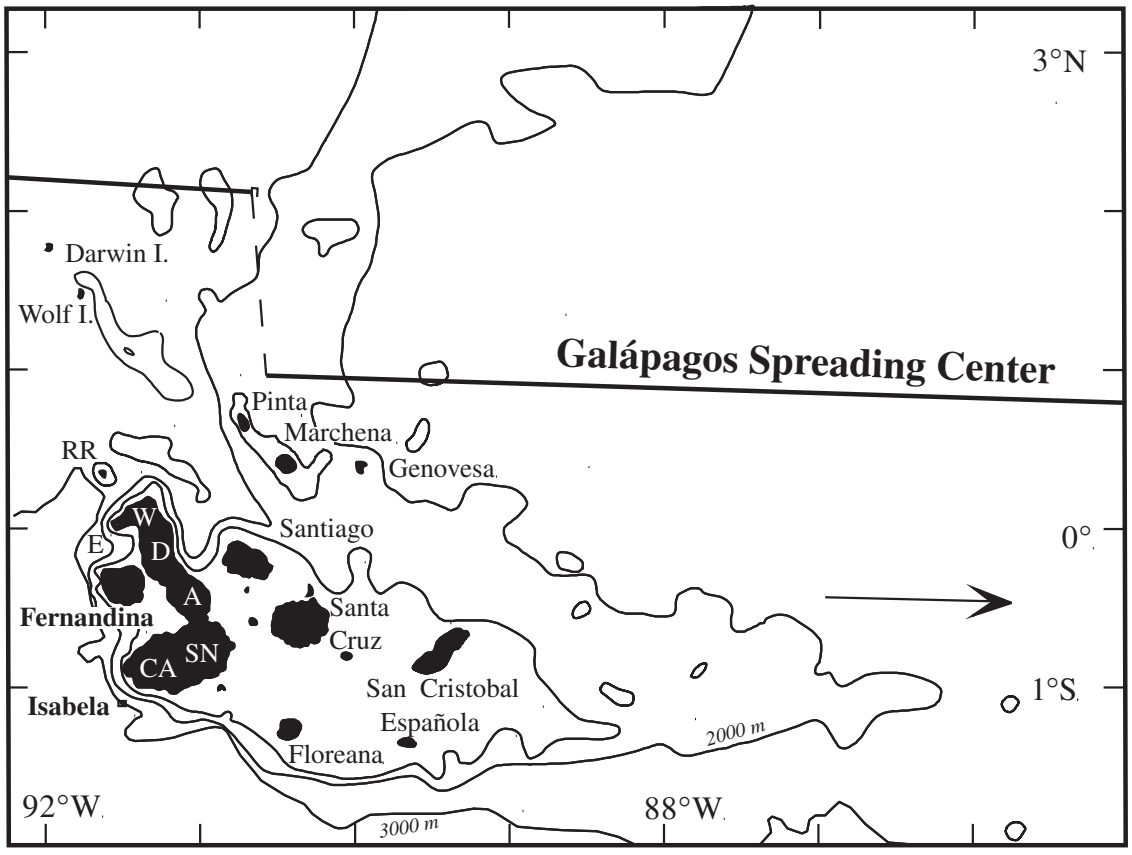

Fig. 1. Map of the Galápagos Islands, showing location of Wolf volcano and the Galápagos Spreading Center. Arrow indicates the absolute motion of the Nazca plate. Volcanoes on Isabela Island are: E, Ecuador; W, Wolf; D, Darwin; A, Alcedo; SN, Sierra Negra; CA, Cerro Azul. RR, Roca Redonda volcano.

unusually depleted Sr, Pb, and Nd isotopic signatures. This paper describes the volcanic history of Wolf volcano for the first time, assesses the petrological processes responsible for the evolution of a remarkably homogeneous suite of basalts, and describes a new model for melting in the upper mantle adjacent to a mantle plume.

GEOLOGICAL DEVELOPMENT OF WOLF VOLCANO

Regional setting

Wolf is one of six shield volcanoes that make up Isabela Island, which along with Fernandina form the western subprovince of the Galápagos Archipelago (Fig. 1). This region is characterized by volcanoes with a distinctive morphology, including 'inverted soup-bowl' cross-sections and deep calderas, as well as frequent volcanic activity, including more than 50 witnessed eruptions (McBirney & Williams, 1969). Recent seismic studies indicate a low-velocity anomaly extending through the upper mantle SW of Fernandina volcano (Toomey *et al.*, 2001), and this anomaly overlies an anomalously thin part of the mantle's Transition Zone (Hooft *et al.*, 2003). The geophysical data thus support geochemical and geochronological evidence that the western Galápagos volcanoes are formed by a deeply rooted mantle plume (e.g. Morgan, 1971; White & Hofmann, 1978; Geist *et al.*, 1988; Graham *et al.*, 1993; White *et al.*, 1993; Sinton *et al.*, 1996; Kurz & Geist, 1999; Harpp & White, 2001).

One of the most notable aspects of volcanoes in the Galápagos is that their isotopic compositions have a systematic spatial distribution (White & Hofmann, 1978) that has been attributed to dynamic mixing between a mantle plume and the upper mantle (Geist *et al.*, 1988; White *et al.*, 1993; Kurz & Geist, 1999; Harpp & White, 2001). The critical observation is that volcanoes of the central part of the archipelago have isotopic compositions within the range of mid-ocean ridge basalts (MORB) from this part of the world, whereas the volcanoes to the north, south, and west have progressively more plume-like isotopic ratios. Wolf volcano has been critical to the development of these models, because it has the most isotopically depleted lavas in the western part of the archipelago (Geist *et al.*, 1988; White *et al.*, 1993).

Wolf volcano lies on lithosphere that is about 10 Myr old, as estimated by extrapolating seafloor magnetic anomalies from outside the archipelago (Wilson & Hey, 1995). It is immediately west and south of a curved boundary that is thought to separate lithosphere that is in Airy compensation to the east and north from lithosphere with an elastic thickness of about 12 km (Feighner & Richards, 1994). Gravity modeling indicates that the crust beneath Wolf volcano is ~11 km thick, although there is a fairly steep gradient in crustal thickness in this area (Feighner & Richards, 1994). Wolf is bordered by young volcanoes to the north (Roca Redonda), west (Ecuador), and south (Darwin), but a >3000 m deep trough lies immediately east of it. Because the absolute motion of the Nazca Plate is 91° (Gripp & Gordon, 1990), this indicates a near absence of volcanism for over a million years in this part of the archipelago before Wolf emerged.

Methods

The subaerial part of Wolf volcano was mapped and samples were collected during a field campaign in 1995, using World War II-era aerial photographs as a base. Multibeam sonar, side scan sonar, and submarine samples (D3 and D4 samples) were collected by dredging during the 2001 DRIFT4 cruise of the R.V. *Roger Revelle* of the Scripps Institution of Oceanography (Fornari *et al.*, 2001; Kurz *et al.*, 2001; Harpp *et al.*, 2002). The MR-1 side-scan sonar system, which is a 11/12 kHz towed system, was used to image the seafloor. The system esonifies the seafloor and collects coregistered backscatter and phasebathymetric data (Rongstadt, 1992; Davis *et al.* 1993). The side-scan data are gridded at 8 m spacing.

Major and trace element analyses were determined by X-ray fluorescence (XRF) at Washington State University according to techniques described by Johnson *et al.* (1999), who reported analyses of international standards. The data and their relative precision, reported as relative standard deviation on a triplicate analysis, are given in Table 1. DRIFT4 glasses were analyzed on the Cameca Camebax electron microprobe at Washington State University. Accelerating voltage was 15 kV. A defocused beam was used, and sodium intensity was monitored as a function of time and corrected for volatilization, although this was not a significant effect. For most samples, two points on three separate shards were measured and averaged. Mineral compositions were determined with the Cameca SX50 microprobe at the University of Hawaii using techniques described by Garcia *et al.* (1995). Rare earth elements (REE) were measured on a subset of samples (Table 2) at Lawrence University by inductively coupled plasma mass spectrometry (ICP-MS); analytical details have been provided by Harpp *et al.* (2003). Helium isotopic compositions (Table 3) were determined at Woods Hole Oceanographic Institution using techniques reported by Kurz & Geist (1999). Magmatic helium isotopic compositions were measured by crushing olivine in a vacuum. The crushed olivine was then fused to release cosmogenic helium for age determinations (Table 4). Argon age measurements (Table 4) were carried out on whole-rock samples by Dr Robert Duncan of Oregon State University using techniques described by Sinton *et al.* (1996). Holocrystalline samples were selected, and groundmass was picked for analysis. Samples were incrementally heated in five 150° steps for measurement of the argon isotopes. Ages are calculated both on isochron and age-spectrum ('plateau') diagrams.

Strontium, lead, and neodymium isotopic analyses were performed at Cornell University and Woods Hole Oceanographic Institution (Table 3). Samples were leached in warm HCl before dissolution to remove salt spray and weathering products. The analyses at Woods Hole were by thermal ionization mass spectrometry (TIMS), and analytical procedures have been reported by Kurz & Geist (1999). Analytical procedures at Cornell have been reported by Blichert-Toft & White (2001), and data for three samples reported in Table 3 were also published in that work. Several of the samples were analyzed in both laboratories, and there is reasonable agreement, but the variability is beyond measurement error in several cases. The differences between the analyses are small compared with the isotopic variation in the region and even Wolf volcano itself. Where duplicate measurements are available, the average values are used for plotting and geochemical modeling.

Geology of Wolf volcano

The most distinctive features of Wolf volcano, as with all Galápagos-type shields, are its shape and the distribution of volcanic vents (Figs 2 and 3). Wolf's vents occur in three clusters: (1) lower, radially distributed flank fissures; (2) arcuate fissures aligned subparallel to the caldera wall; (3) caldera floor vents (Figs 2 and 3). The radial fissures are concentrated in three zones that extend north, NW, and SE of the summit (Fig. 3). Young submarine vents are identified in the bathymetric and side-scan sonar data and form ridges that extend seaward from the north and NW subaerial vent clusters (Figs 2 and 3). In the submarine environment, the vents form more sharply delineated ridges than on the subaerial part of the volcano. The mottled texture on the side-scan sonar image is a likely indication of pillow lavas and mounds separated by fragmental debris and sediment.

The subaerial clusters of fissures are unlike Hawaiian and Icelandic rift zones because they are much less focused, hence they are referred to as 'diffuse rift zones' (Geist *et al.*, 2003), and they impart asymmetry to the volcano (Fig. 2). The NW and north diffuse rifts extend

Table 1: Major and trace element analyses of Wolf lavas

	W95 1	W95 2	W95 3	W95 4	W95 5	W95 6	W95 7	W95 8	W95 9	W95 10	W95 11	W95 12
Lat. (0°):	−·05	·0028	·02	·03	·0309	·0311	·0266	·021	·0163	·0088	−·001	−·002
Long. (91°W):	·41	·3619	·37	·33	·3230	·3230	·3206	·319	·3166	·3175	·325	·327
Unit:	Fuv	Ry	H(1984)	Ry	Ry	Ry	Ry	Ry	Ry	Ry	Ry	Ry
SiO_2	48·97	49·42	49·18	49·13	49·35	48·51	48·84	49·53	49·26	49·38	49·12	50·02
Al_2O_3	14·69	14·49	15·65	14·23	14·33	14·42	13·95	14·29	14·33	14·30	14·32	14·67
TiO_2	3·21	3·22	2·71	3·23	3·21	3·25	3·33	3·31	3·09	3·10	3·09	3·05
FeO	11·78	11·76	10·47	11·64	12·07	11·48	12·52	11·76	11·81	11·86	11·74	11·05
MnO	0·19	0·19	0·17	0·19	0·19	0·20	0·20	0·19	0·19	0·19	0·19	0·18
CaO	10·75	11·00	11·85	10·87	10·86	10·92	10·40	10·69	11·17	11·18	11·18	11·04
MgO	6·28	6·17	6·40	6·11	6·16	6·27	5·69	6·05	6·33	6·43	6·28	6·70
K_2O	0·56	0·54	0·44	0·57	0·54	0·54	0·56	0·58	0·52	0·52	0·52	0·50
Na_2O	3·26	3·42	3·03	3·44	3·28	3·19	3·42	3·45	3·05	3·10	3·10	3·18
P_2O_5	0·40	0·38	0·31	0·39	0·39	0·39	0·41	0·41	0·34	0·34	0·34	0·36
Total	100·09	100·59	100·22	99·81	100·38	99·16	99·32	100·26	100·09	100·41	99·89	100·75
Mg-no.	48·7	48·3	52·1	48·3	47·6	49·3	44·8	47·8	48·9	49·2	48·8	51·9
Sc	46	49	46	39	35	31	30	29	33	30	35	33
V	371	376	310	366	368	370	377	369	372	382	382	358
Ba	91	112	88	94	114	115	116	114	113	116	108	99
Rb	5	5	5	7	7	5	6	6	5	5	6	6
Sr	376	384	391	380	380	376	353	380	388	392	387	375
Zr	236	224	189	236	234	232	242	247	207	205	205	220
Y	35	34	29	36	36	35	37	37	31	31	31	33
Nb	19	18	15	19	19	18	19	20	18	17	17	16
Ga	24	21	21	24	23	20	24	24	23	20	22	22
Cu	95	88	100	76	73	228	76	80	102	100	105	109
Zn	100	103	87	102	96	104	110	105	97	98	101	94

	W95 13	W95 14	W95 15	W95 16	W95 17	W95 18	W95 19	W95 20	W95 21	W95 22	W95 23	W95 24
Lat. (0°):	−·0058	−·0058	−·0079	−·0053	−·0055	−·0055	−·0055	·003	·0032	·003	·003	.006
Long. (91°W):	.3514	·3514	·3462	·3487	·3395	·3395	·3395	·361	·3612	·361	·361	·359
Unit:	Ry	Ry	Ry	Ry	Fy	Ry	Ry	Ry	Ry	Ry	Ry	Cf
SiO_2	48·62	48·92	48·80	48·39	49·35	48·95	49·36	48·53	48·69	48·52	48·23	48·97
Al_2O_3	14·27	14·00	14·46	14·40	14·02	14·27	14·17	14·24	13·96	13·92	17·15	16·96
TiO_2	3·04	3·44	2·99	3·26	3·62	3·23	3·54	3·05	3·31	2·77	2·34	2·90
FeO	11·88	12·14	11·22	11·64	12·24	11·42	11·87	11·30	12·38	11·06	9·21	10·39
MnO	0·19	0·20	0·18	0·19	0·20	0·19	0·20	0·19	0·20	0·19	0·14	0·17
CaO	11·20	10·39	11·29	10·92	10·18	10·90	10·42	11·09	10·60	11·92	12·18	11·38
MgO	6·34	5·78	6·51	6·04	5·57	6·04	5·74	6·26	5·97	6·60	6·21	4·90
K_2O	0·51	0·60	0·54	0·57	0·63	0·57	0·60	0·50	0·54	0·40	0·30	0·49
Na_2O	2·99	3·25	3·62	3·36	3·62	3·28	3·38	3·16	3·24	2·95	2·42	3·18
P_2O_5	0·34	0·42	0·57	0·48	0·45	0·40	0·43	0·36	0·38	0·29	0·24	0·34
Total	99·39	99·14	100·19	99·25	99·88	99·24	99·70	98·68	99·27	98·62	98·42	99·68
Mg-no.	48·8	45·9	50·8	48·1	44·8	48·5	46·3	49·7	46·2	51·5	54·6	45·7

	W95 13	W95 14	W95 15	W95 16	W95 17	W95 18	W95 19	W95 20	W95 21	W95 22	W95 23	W95 24
Lat. (0°):	−·0058	−·0058	−·0079	−·0053	−·0055	−·0055	−·0055	·003	·0032	·003	·003	·006
Long. (91°W):	.3514	·3514	·3462	·3487	·3395	·3395	·3395	·361	·3612	·361	·361	·359
Unit:	Ry	Ry	Ry	Ry	Fy	Ry	Ry	Ry	Ry	Ry	Ry	Cf
Sc	36	37	40	34	34	33	32	35	36	39	28	30
V	385	395	359	372	390	381	388	352	390	378	272	334
Ba	125	131	127	125	125	122	124	98	118	90	83	108
Rb	5	7	7	5	6	5	6	6	5	4	3	6
Sr	391	376	388	389	376	385	376	388	389	317	382	415
Zr	207	249	209	241	272	238	258	218	238	180	154	211
Y	31	37	31	33	41	35	38	32	36	33	23	32
Nb	17	20	17	20	20	19	21	17	17	13	11	15
Ga	26	22	21	20	23	22	23	24	25	20	19	20
Cu	99	122	108	51	107	90	92	74	112	†153	82	89
Zn	98	106	93	94	108	94	96	93	103	87	70	89

	W95 25	W95 26	W95 27	W95 28	W95 29	W95 30	W95 31	W95 32	W95 33	W95 34	W95 35	W95 36
Lat. (0°):	·008	·0080	·008	·0086	·0120	·0120	·0057	·0025	·003	·003	·003	·003
Long. (91°W):	·357	·3573	·357	·3568	·3539	·3539	·3657	·3665	·367	·367	·367	·366
Unit:	Cf	Cf	Cf	Cr	Cf	H(1982)	Ry	Ry	Ry	Ry	Ry	Ry
SiO_2	49·36	48·63	49·21	49·15	49·31	48·75	48·77	48·87	49·00	49·23	48·85	48·31
Al_2O_3	16·58	14·68	14·22	14·34	16·77	15·51	14·25	16·24	15·42	14·25	14·15	14·14
TiO_2	2·52	2·96	3·30	3·16	2·94	2·73	3·02	2·71	2·86	3·21	3·12	3·13
FeO	9·90	11·81	11·58	11·88	10·33	10·45	12·01	9·65	10·58	11·98	12·08	11·51
MnO	0·16	0·19	0·19	0·19	0·17	0·17	0·19	0·17	0·18	0·19	0·19	0·19
CaO	12·05	11·35	10·88	11·03	11·48	11·84	11·17	11·62	11·84	10·65	10·76	10·77
MgO	6·07	6·18	6·11	6·23	5·26	6·26	6·36	5·72	6·56	5·95	6·02	6·00
K_2O	0·38	0·43	0·52	0·50	0·49	0·44	0·52	0·46	0·41	0·56	0·54	0·52
Na_2O	2·91	3·02	3·25	3·22	3·16	3·01	3·07	3·10	2·95	3·35	3·25	3·21
P_2O_5	0·28	0·31	0·38	0·36	0·35	0·31	0·34	0·34	0·32	0·41	0·39	0·38
Total	100·21	99·56	99·64	100·06	100·26	99·47	99·70	98·88	100·12	99·79	99·36	98·16
Mg-no.	52·2	48·3	48·5	48·3	47·6	51·6	48·6	51·4	52·5	47·0	47·0	48·2
Sc	36	40	36	37	32	38	37	38	39	34	36	37
V	316	361	378	364	316	324	359	319	335	380	361	362
Ba	89	112	106	106	96	94	107	99	82	105	108	107
Rb	5	5	6	5	5	5	5	5	4	7	4	6
Sr	390	370	371	379	410	390	386	407	364	373	373	384
Zr	173	192	231	222	214	188	208	202	194	252	236	233
Y	28	30	36	34	32	30	31	31	32	38	37	35
Nb	14	15	17	16	16	15	18	16	14	19	18	16
Ga	22	22	22	19	24	20	23	21	19	24	23	19
Cu	98	130	121	108	94	102	101	111	113	104	84	79
Zn	78	98	99	99	†128	86	98	92	91	105	100	98

Table 1: continued

	W95 37	W95 38	W95 39	W95 40	W95 41	W95 42	W95 43	W95 44	W95 45	W95 46	W95 47	W95 48
Lat. (0°):	·003	·003	·0084	·0084	·0097	·0172	·017	·017	·0167	·0167	·016	·0163
Long. (91°W):	·366	·366	·3607	·3607	·3618	·3642	·364	·364	·3648	·3648	·365	·3656
Unit:	Ry	Ry	Cf	Cf	Cf	dike	Ro	Ro	Ro	Ro	Ro	Ry
SiO_2	48·55	48·96	48·52	46·13	48·89	49·09	48·96	48·86	49·75	48·33	48·63	48·02
Al_2O_3	14·33	14·56	13·95	13·55	14·31	14·28	13·98	15·57	13·92	14·25	14·32	14·22
TiO_2	3·23	3·06	3·71	3·18	3·02	3·15	3·35	2·81	3·48	3·10	3·21	3·02
FeO	11·85	11·69	13·18	11·39	11·99	11·76	12·11	10·82	12·30	11·32	11·68	11·45
MnO	0·19	0·18	0·21	0·19	0·19	0·19	0·19	0·17	0·21	0·19	0·18	0·19
CaO	10·72	11·13	9·76	10·38	11·20	10·41	10·69	11·59	9·36	11·07	10·96	11·22
MgO	6·00	6·39	5·16	5·69	6·40	5·71	5·78	6·12	5·04	6·02	6·06	6·48
K_2O	0·55	0·49	0·64	0·54	0·51	0·66	0·57	0·42	0·81	0·45	0·47	0·44
Na_2O	3·40	3·27	3·57	3·04	3·03	3·29	3·16	3·01	3·55	2·88	3·02	3·06
P_2O_5	0·39	0·35	0·49	0·38	0·34	0·44	0·40	0·33	0·68	0·36	0·37	0·34
Total	99·21	100·09	99·19	94·46	99·89	98·98	99·19	99·71	99·10	97·96	98·90	98·43
Mg-no.	47·4	49·4	41·1	47·1	48·8	46·4	46·0	50·2	42·2	48·7	48·1	50·2
Sc	35	40	35	36	39	39	40	33	31	34	35	39
V	373	367	395	376	360	355	374	312	352	339	340	323
Ba	121	82	122	81	84	110	96	95	151	102	104	97
Rb	7	5	7	7	6	6	4	3	10	3	4	5
Sr	388	387	379	387	388	382	353	356	349	361	370	372
Zr	235	213	279	231	207	265	238	201	385	223	229	215
Y	36	32	42	35	31	39	37	34	58	36	35	33
Nb	19	17	23	19	17	21	19	15	29	17	16	15
Ga	21	24	24	23	21	25	26	21	27	24	21	21
Cu	76	109	95	113	97	104	116	113	93	105	101	86
Zn	100	93	111	100	96	105	102	93	†121	98	94	97

	W95 49	W95 50	W95 51	W95 52	W95 53	W95 54	W95 55	W95 56	W95 57	W95 58	W95 59	W95 60
Lat. (0°):	·016	−·0416	−·0420	−·0420	−·0633	−·05	−·051	−·051	−·052	−·052	−·06	−·06
Long. (91°W):	·366	·3885	·3885	·3885	·4083	·41	·39	·38	·37	·37	·41	·41
Unit:	Ry	Ry	Fv	Fv	Fv	Fuv	Fuv	Fuv	Fuv	Fv	Fv	Fuv
SiO_2	48·00	48·16	49·04	48·59	49·13	48·67	47·86	48·48	48·32	48·72	48·97	48·74
Al_2O_3	14·08	14·05	13·98	16·14	14·35	14·28	13·85	14·44	13·82	13·98	15·20	17·12
TiO_2	3·19	3·03	3·41	2·61	3·11	3·25	3·48	3·10	3·43	3·40	2·90	2·85
FeO	12·01	12·08	12·10	10·01	11·81	11·86	12·41	11·85	12·17	12·17	10·69	10·69
MnO	0·19	0·19	0·19	0·16	0·19	0·19	0·20	0·19	0·20	0·19	0·18	0·17
CaO	10·84	11·04	10·35	11·91	11·02	10·56	10·30	11·02	10·13	10·34	11·38	11·42
MgO	6·04	6·19	5·68	6·07	6·18	5·95	5·54	6·27	5·60	5·65	6·42	4·69
K_2O	0·47	0·51	0·63	0·45	0·49	0·57	0·58	0·49	0·59	0·64	0·47	0·40
Na_2O	3·19	3·03	3·27	2·88	2·93	3·20	3·26	3·09	3·29	3·25	2·97	3·02
P_2O_5	0·37	0·34	0·42	0·31	0·36	0·40	0·43	0·36	0·42	0·42	0·34	0·28
Total	98·38	98·62	99·07	99·13	99·57	98·93	97·91	99·29	97·96	98·76	99·53	99·39
Mg-no.	47·3	47·7	45·6	51·9	48·3	47·2	44·3	48·5	45·1	45·3	51·7	43·9

	W95 49	W95 50	W95 51	W95 52	W95 53	W95 54	W95 55	W95 56	W95 57	W95 58	W95 59	W95 60
Lat. (°):	·016	−·0416	−·0420	−·0420	−·0633	−·05	−·051	−·051	−·052	−·052	−·06	−·06
Long. (91°W):	·366	·3885	·3885	·3885	·4083	·41	·39	·38	·37	·37	·41	·41
Unit:	Ry	Ry	Fv	Fv	Fv	Fuv	Fuv	Fuv	Fuv	Fv	Fv	Fuv
Sc	37	34	36	31	36	33	38	37	36	36	37	30
V	348	359	378	312	362	373	399	363	395	382	332	359
Ba	97	123	123	80	101	113	131	105	121	117	95	85
Rb	3	5	6	6	4	7	5	5	6	4	5	4
Sr	355	388	381	396	379	373	377	380	363	378	380	389
Zr	228	209	247	187	220	241	254	220	252	245	205	173
Y	37	31	38	28	33	37	39	33	38	37	32	28
Nb	17	18	21	14	17	20	20	17	20	19	16	16
Ga	22	24	24	21	26	23	25	24	25	24	20	24
Cu	114	106	117	115	121	96	126	123	92	112	118	121
Zn	95	97	105	82	101	99	107	94	104	103	98	93

	W95 61	W95 62	W95 63	W95 64	W95 65	W95 66	W95 67	W95 68	W95 69	W95 70	W95 71	W95 72
Lat. (°):	−·06	−·06	−·08	·12	·12	·12	·12	·1386	·1379	·1315	·0803	·0753
Long. (91°W):	·41	·41	·41	·42	·42	·42	·42	·3742	·3768	·3523	·2933	·2905
Unit:	Fv	Fv	Fuv	Fuv	Fv	Fv	Fv	Fuv	Fv	Fuv	Fv	Fuv
SiO_2	47·77	48·61	48·27	49·12	48·91	48·95	48·68	49·12	48·35	48·82	49·27	48·95
Al_2O_3	15·51	17·23	14·26	16·76	14·02	18·36	14·60	15·29	16·10	17·76	16·71	17·78
TiO_2	3·16	1·61	3·47	2·75	3·46	2·53	3·33	3·19	3·01	2·58	2·56	2·45
FeO	11·94	7·79	12·77	9·98	12·06	9·15	11·91	11·35	11·17	9·96	9·48	9·39
MnO	0·18	0·13	0·20	0·16	0·20	0·15	0·20	0·19	0·18	0·16	0·16	0·15
CaO	9·75	12·74	10·59	11·59	10·24	11·94	10·45	10·80	11·06	11·79	11·79	12·17
MgO	7·28	9·50	5·57	5·60	5·72	4·86	5·83	5·59	5·38	5·19	5·57	5·40
K_2O	0·57	0·25	0·48	0·50	0·60	0·44	0·57	0·49	0·45	0·40	0·42	0·40
Na_2O	3·16	2·16	3·17	3·22	3·45	3·18	3·50	3·32	3·10	3·01	2·92	2·90
P_2O_5	0·37	0·19	0·33	0·34	0·44	0·31	0·41	0·38	0·36	0·30	0·31	0·29
Total	99·69	100·21	99·11	100·03	99·09	99·87	99·48	99·72	99·16	99·97	99·19	99·89
Mg-no.	52·1	68·5	43·7	50·0	45·8	48·6	46·6	46·8	46·2	48·2	51·2	50·6
Sc	32	34	38	36	32	32	33	34	33	32	38	35
V	342	204	434	311	391	294	364	348	338	287	290	289
Ba	173	34	110	81	135	86	117	112	106	103	85	81
Rb	8	5	6	5	5	6	6	6	5	4	4	4
Sr	378	359	354	409	379	431	383	392	404	415	380	396
Zr	193	118	204	213	251	186	240	226	218	191	186	178
Y	33	18	35	32	40	27	36	34	34	29	30	27
Nb	24	9	19	16	21	15	19	19	19	14	14	13
Ga	24	19	23	24	24	24	24	24	24	22	25	21
Cu	46	58	144	88	117	85	97	100	99	73	81	84
Zn	112	56	109	85	103	75	101	96	97	81	85	78

Table 1: continued

	W95 73	W95 74	W95 75	W95 76	W95 77	W95 78	W95 79	W95 80	W95 81	W95 82	W95 83	W95 84
Lat. (0°):	·0753	·0691	·0672	·0608	·0608	·10	·10	·09	·09	·09	·08	·08
Long. (91°W):	·2905	·2944	·2874	·2913	·2910	·30	·30	·30	·30	·30	·30	·30
Unit:	Fv	Fuv	Fuv	Ry	Fv	Fv	Fuv	Fuv	Fv	Fv	Fv	Fuv
SiO_2	48·93	48·86	49·36	48·86	48·96	48·19	49·35	49·37	49·73	49·50	48·77	48·85
Al_2O_3	13·71	18·10	18·37	14·46	14·43	17·70	14·23	14·30	14·78	14·01	14·29	15·18
TiO_2	3·74	2·32	2·32	3·21	3·25	2·16	3·45	3·25	3·15	3·73	3·13	2·73
FeO	13·47	8·99	8·91	11·63	11·71	8·67	12·33	11·77	11·61	12·77	11·84	10·53
MnO	0·21	0·14	0·14	0·19	0·19	0·14	0·20	0·19	0·19	0·21	0·19	0·17
CaO	9·63	12·45	12·50	10·91	10·74	12·44	10·39	10·70	10·85	9·66	10·99	10·90
MgO	5·14	5·75	5·91	6·15	6·04	7·05	5·76	6·06	6·21	5·21	6·28	7·91
K_2O	0·65	0·39	0·37	0·54	0·56	0·37	0·60	0·57	0·54	0·68	0·51	0·48
Na_2O	3·51	2·89	2·76	3·22	3·17	2·67	3·44	3·29	3·23	3·62	3·23	2·94
P_2O_5	0·48	0·28	0·29	0·39	0·39	0·25	0·43	0·39	0·38	0·49	0·37	0·34
Total	99·47	100·17	100·93	99·56	99·44	99·65	100·17	99·89	100·67	99·88	99·59	100·04
Mg-no.	40·5	53·3	54·2	48·5	47·9	59·2	45·4	47·9	48·8	42·1	48·6	57·3
Sc	36	31	35	34	37	33	32	34	34	33	39	37
V	419	270	273	363	374	257	402	364	379	420	358	330
Ba	149	78	82	110	115	74	110	108	109	145	93	97
Rb	9	4	3	4	6	5	5	7	7	7	4	5
Sr	371	420	418	382	388	406	373	381	386	363	383	360
Zr	276	172	170	231	233	158	254	233	228	283	218	200
Y	43	27	27	37	34	23	39	35	34	44	34	31
Nb	22	13	13	20	19	12	20	19	19	21	17	16
Ga	24	23	21	24	24	21	24	24	25	23	22	24
Cu	88	76	78	79	116	81	123	123	115	95	117	88

	W95 85	W95 86	D3A	D4C	D4E	D4F	D4A	D4B	RSD%
Lat. (0°):	·0171	·02	·2667	·1900	·1900	·1900	·1900	·1900	
Long. (91°W):	·2178	·22	·4333	·4128	·4128	·4128	·4128	·4128	
Unit:	Fv	Fy	Sub	Sub	Sub	Sub	Sub	Sub	
SiO_2	47·97	48·97	48·06	48·90	48·75	48·59	48·66	48·82	0·4
Al_2O_3	13·67	15·67	15·04	13·56	14·02	13·57	13·39	13·60	0·3
TiO_2	3·47	2·71	3·12	4·16	3·63	4·18	4·14	4·05	0·2
FeO	12·08	10·35	10·73	13·04	12·19	13·17	13·61	13·27	1·9
MnO	0·20	0·17	0·17	0·21	0·21	0·24	0·20	0·21	0·3
CaO	10·95	11·54	11·48	9·91	10·66	9·98	9·61	9·80	0·1
MgO	5·56	6·64	6·33	5·02	5·60	5·06	5·06	5·00	1·8
K_2O	0·54	0·43	0·56	0·72	0·67	0·72	0·77	0·74	0·0
Na_2O	3·18	3·00	3·93	3·44	3·58	3·60	3·54	3·52	0·9
P_2O_5	0·42	0·33	0·31	0·39	0·50	0·51	0·50	0·47	0·6
Total	98·05	99·81	99·72	99·55	99·54	99·52	99·51	99·49	
Mg-no.	45·1	53·4	51·3	45·0	40·2	39·8	40·6	40·7	
Sc	30	33							3·1

	W95 85	W95 86	D3A	D4C	D4E	D4F	D4A	D4B	RSD%
Lat. (0°):	·0171	·02	·2667	·1900	·1900	·1900	·1900	·1900	
Long. (91°W):	·2178	·22	·4333	·4128	·4128	·4128	·4128	·4128	
Unit:	Fv	Fy	Sub	Sub	Sub	Sub	Sub	Sub	
V	388	302							1·8
Ba	118	78							2·7
Rb	7	4							10·5
Sr	393	378							0·1
Zr	251	194							0·3
Y	40	31							2·0
Nb	19	15							4·4
Ga	23	21							5·0
Cu	123	100							2·3
Zn	107	91							2·3

Samples with W95 prefix are by XRF; samples with D prefix are electron microprobe analyses of glasses. Locations with four significant figures were measured by global positioning system, and others estimated from aerial photographs. Here, flank lavas are broken into two divisions, on the basis of the extent of vegetation: H, historical; Fuv, unvegetated flank lava; Fv, vegetated flank lava; Ry, young flow from circumferential fissure; Cf, caldera-filling facies lava; Ro, rim facies lava older than caldera fill.

Table 2: Rare earth element concentrations of Wolf lavas

Sample	La	Ce	Pr	Nd	Sm	Eu	Gd	Tb	Dy	Ho	Er	Tm	Yb	Lu
W95-59	15·8	39·2	5·7	26·8	6·88	2·26	7·15	1·10	6·22	1·19	3·12	0·42	2·56	0·39
W95-33	13·9	35·4	5·3	25·5	6·72	2·23	7·17	1·12	6·38	1·23	3·21	0·44	2·67	0·41
W95-45	27·4	70·0	10·3	48·3	12·2	3·69	12·7	1·93	11·01	2·12	5·57	0·75	4·67	0·71
W95-54	18·5	46·2	6·7	31·3	7·88	2·53	8·16	1·27	7·14	1·38	3·62	0·50	3·04	0·46
W95-55	20·1	50·1	7·3	34·0	8·57	2·78	8·91	1·37	7·71	1·48	3·89	0·54	3·22	0·49
W95-63	38·7	27·5	22·5	16·4	17·0	4·66	4·88	4·29	3·90	3·96	2·34	1·93	1·66	1·65
W95-74	12·5	31·5	4·7	22·1	5·69	1·96	6·00	0·94	5·27	1·01	2·65	0·37	2·19	0·33
W95-75	15·2	38·1	5·6	26·2	6·63	2·16	6·86	1·07	6·03	1·15	3·03	0·42	2·53	0·39
W95-84	15·2	38·1	5·6	26·2	6·63	2·16	6·86	1·07	6·03	1·15	3·03	0·42	2·53	0·39

the salients on the northern part of the island, creating a concave northern coast. The NW diffuse rift extends to Roca Redonda (Fig. 2, bottom), a 3000 m high, mostly submarine volcano (Standish *et al.*, 1998). The SE diffuse rift extends to the flanks of Volcan Darwin (Naumann *et al.*, 2003). The NW and SE diffuse rifts support the hypothesis of Chadwick & Howard (1991) that loading by adjacent volcanoes combined with stresses exerted by pressurized subcaldera magma bodies guide dikes towards those volcanoes. Each of the three sectors that has a diffuse rift zone also has the lowest slope gradients on the volcano (Mouginis-Mark *et al.* 1996), indicating that the concentration of vents in these diffuse rift zones has persisted over the long-term growth of the edifice. Likewise, the two steepest flanks of the volcano, the east and west flanks, have few satellite vents.

Lavas erupted from Wolf's radial fissures are dominantly large-volume a'a flows. Wolf is covered almost entirely with a'a, and, in our experience, has more a'a lava than any other Galápagos volcano. This is partly because of the large proportion of unusually steep slopes that make up the upper flanks of Wolf volcano, which is conducive to a'a formation. Also, flows from the radial vents tend to be more voluminous than flows erupted

Table 3: Isotopic ratios of selected Wolf lavas

	R/R_a	±
W95-25	8·64	0·15
W95-54	9·83	0·05
W95-59	9·04	0·06
W95-74	8·89	0·12
W95-75	8·58	0·10
W95-84	9·22	0·15

Sample	$^{87}Sr/^{86}Sr$ Cornell	±	$^{87}Sr/^{86}Sr$ WHOI	±	$^{143}Nd/^{144}Nd$ Cornell	±	$^{143}Nd/^{144}Nd$ WHOI	±	$^{206}Pb/^{204}Pb$ Cornell	±	$^{206}Pb/^{204}Pb$ WHOI	±	$^{207}Pb/^{204}Pb$ Cornell	±	$^{207}Pb/^{204}Pb$ WHOI	±	$^{208}Pb/^{204}Pb$ Cornell	±	$^{208}Pb/^{204}Pb$ WHOI	±
W95-25	0·70270*	1	0·70277	2	0·513056*	12	0·513032	14	18·919*	9	18·868	10	15·535*	12	15·557	14	38·366*	40	38·423	16
W95-59	0·70274*	1			0·513049*	12			18·975*	9			15·546*	12			38·439*	40		
W95-61	0·70310	1			0·512987	12														
W95-74	0·70271*	1	0·70277	2	0·513048*	12	0·513035	10	18·885*	9	18·895	10	15·573*	12	15·558	14	38·563*	40	38·452	16
W95-84	0·70274	1	0·70275	2	0·513037	12	0·513034	12			18·897	10			15·542	14			38·377	16
W95-54			0·70274	2			0·513023	10			18·889	10			15·541	14			38·373	16
W95-75			0·70276	2			0·513031	10												

$^{87}Sr/^{86}Sr$ has been normalized to a value of 0·71024 for NBS987 and $^{143}Nd/^{144}Nd$ to 0·51184 for the La Jolla standard. Helium isotopic ratios (units of R/R_a) have been determined by crushing olivine grains in a vacuum.
*Data reported by Blichert-Toft & White (2001).

Table 4: Age determinations on lavas from Wolf Volcano

Sample	Elevation (m)	Age (ka)	±	Method
W95-38	1598	20	22	$^{39}Ar/^{40}Ar$ plateau
W95-43	1420	173	20	$^{39}Ar/^{40}Ar$ plateau
		71	33	$^{39}Ar/^{40}Ar$ isochron
W95-74	3	<1		^{3}He
W95-84	5	<0·5		^{3}He
W95-59	6	1·8	0·8	^{3}He
W95-25	1363	<0·2		^{3}He
W95-75	2	<0·5		^{3}He

Argon analyses completed on groundmass separates. ^{3}He surface exposure ages of olivine separates calculated using production rates and altitude scaling described by Kurz & Geist (1999).

from the summit region, suggesting relatively high eruption rates, which also favor the formation of a'a over pahoehoe (Rowland & Walker, 1990; Naumann & Geist, 2000).

For reasons that remain unclear, the submarine rifts at Wolf volcano are much more focused than the subaerial rifts, creating sharper ridges in the submarine environment than in the subaerial setting (Figs 2 and 3). The same phenomenon occurs at Fernandina volcano (Kurz *et al.*, 2001) and must be a consequence of lavas erupting from several closely spaced fissures instead of over zones several kilometers wide. Also, on the basis of the submarine samples dredged from the northern flanks of Wolf volcano, it is likely that the primary lava morphology on these submarine rifts is pillow basalts, usually indicative of lower effusion rates (Gregg & Fink, 1995), hence forming short, stubby flows.

Lavas on the summit platform (a 100–400 m wide plateau between the caldera wall and steep outer flanks) are dominantly small-volume pahoehoe flows erupted from fissures subparallel to the caldera wall (Figs 3 and 4). Some of the flows that traversed the platform and spilled over the caldera walls have curious 'lava crevasses' that form perpendicular to the flow direction (parallel to the lip of the caldera wall) but are 50–100 m away from the caldera wall. By analogy to similar glacial features, we believe that these form after the lava has developed a thick brittle crust, and the drag of the flow front down the vertical caldera wall causes slow plastic flow of the hot interior, tearing cracks in the solidified flow top. The caldera floor is mostly covered by a sheet-like a'a flow that erupted in 1982. The vent is situated low on the SW caldera wall at the base of the bench. Photos taken during the eruption (T. de Roy, personal communication, 2000) show that the flow advanced as a single broad sheet, and that it was ~5 m thick.

Geology of the caldera: caldera floor vs caldera rim facies

Wolf volcano's caldera is 700 m deep and 6 km by 5 km in plan view (Fig. 4). The caldera wall contains outcrops of older lavas, the only such exposures on the volcano; erosion rates are so slow that rocks older than a few thousand years are almost never exposed on the western Galápagos shields (Kurz & Geist, 1999). The most prominent feature within the caldera is a 4 km × 1 km bench perched 450 m above the western caldera floor (Fig. 4). The substrate of the bench is a series of massive, mostly flat, a'a lava flows, each ~2 m to 6 m thick.

Lavas exposed in the southern caldera wall are of two types. Below ~450 m above the caldera floor, they are thick and massive, like those exposed below the western bench (Fig. 4). Above 450 m, they are thin (typically 0·5–2 m thick) and mostly pahoehoe. The lower lavas are laterally extensive (single flows are traceable for several kilometers), whereas the upper units appear to extend laterally for less than ~200 m. Similar lava flow sequences have now been observed in the walls of Cerro Azul (Naumann & Geist, 2000) and Fernandina volcanoes (Rowland & Munro, 1992) and in the uplifted fault block at Sierra Negra volcano (Reynolds *et al.*, 1995). Owing to textural and dimensional similarities to recent lavas whose origin is known, the two types of lava are referred to as 'caldera-filling facies' and 'caldera rim facies'. Caldera-filling lava flows are several meters thick and have undergone large-scale vesicle segregation because they ponded on the caldera floor; a typical example is the 1982 flow. In contrast, most caldera rim lava flows are thin, have pahoehoe surfaces, and form at relatively low eruption rates.

Our interpretation of the distribution of the different facies around the caldera wall is that an older caldera filled partly, to 450 m above the current caldera floor. The western bench represents a remnant of this older caldera floor. This was followed by a second stage of collapse that was smaller in diameter and off-center of the earlier caldera. Since the renewed collapse, summit growth has occurred by the eruption of lava from circumferential fissures at the caldera rim, producing a second phase of younger caldera rim facies.

The southern floor of Wolf caldera is covered by voluminous avalanche deposits from several major failures of the caldera wall (Fig. 4). All of these deposits are unconformably overlain by 1982 lava. Satellite radar interferometry (InSAR) shows that the largest avalanche deposits subsided ~11 cm between 1992 and 1998 (Amelung *et al.*, 2000), a rate of 17 mm/year. This subsidence is probably the result of sediment compaction, and such active subsidence indicates that the largest of the avalanches must be relatively young. A similarly large avalanche was associated with the 1989 eruption of Fernandina (Chadwick

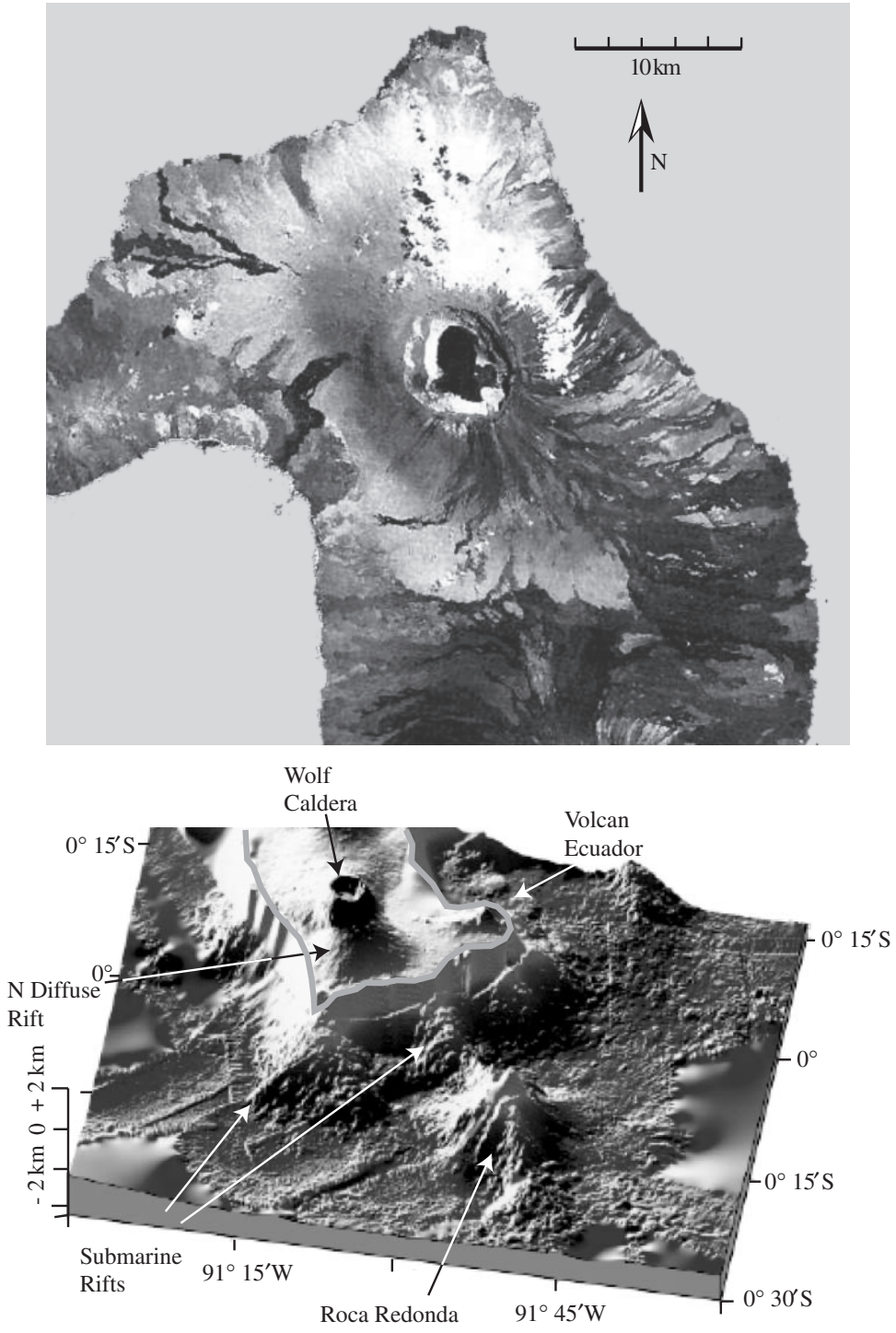

Fig. 2. Top: Landsat7 image of Wolf volcano, showing the distribution of young, unvegetated lava flows. Bottom: perspective of relief of submarine and subaerial sectors, looking from the NE. Data are merged bathymetry and side-scan sonar from the DRIFT4 cruise and subaerial DEM produced from radar data of the TOPSAR mission (Mouginis-Mark *et al.*, 1996; data kindly provided by P. Mouginis-Mark).

et al., 1991), suggesting that large-scale mass wasting well after caldera collapse is a common erosional process related to the evolution of calderas in Galápagos volcanoes.

The western sector of the caldera wall exposes dozens of thin (0·5–1 m wide) dikes that strike subparallel to the caldera wall. As has now been observed at several of the western shield volcanoes (Ecuador: Geist *et al.*, 2002;

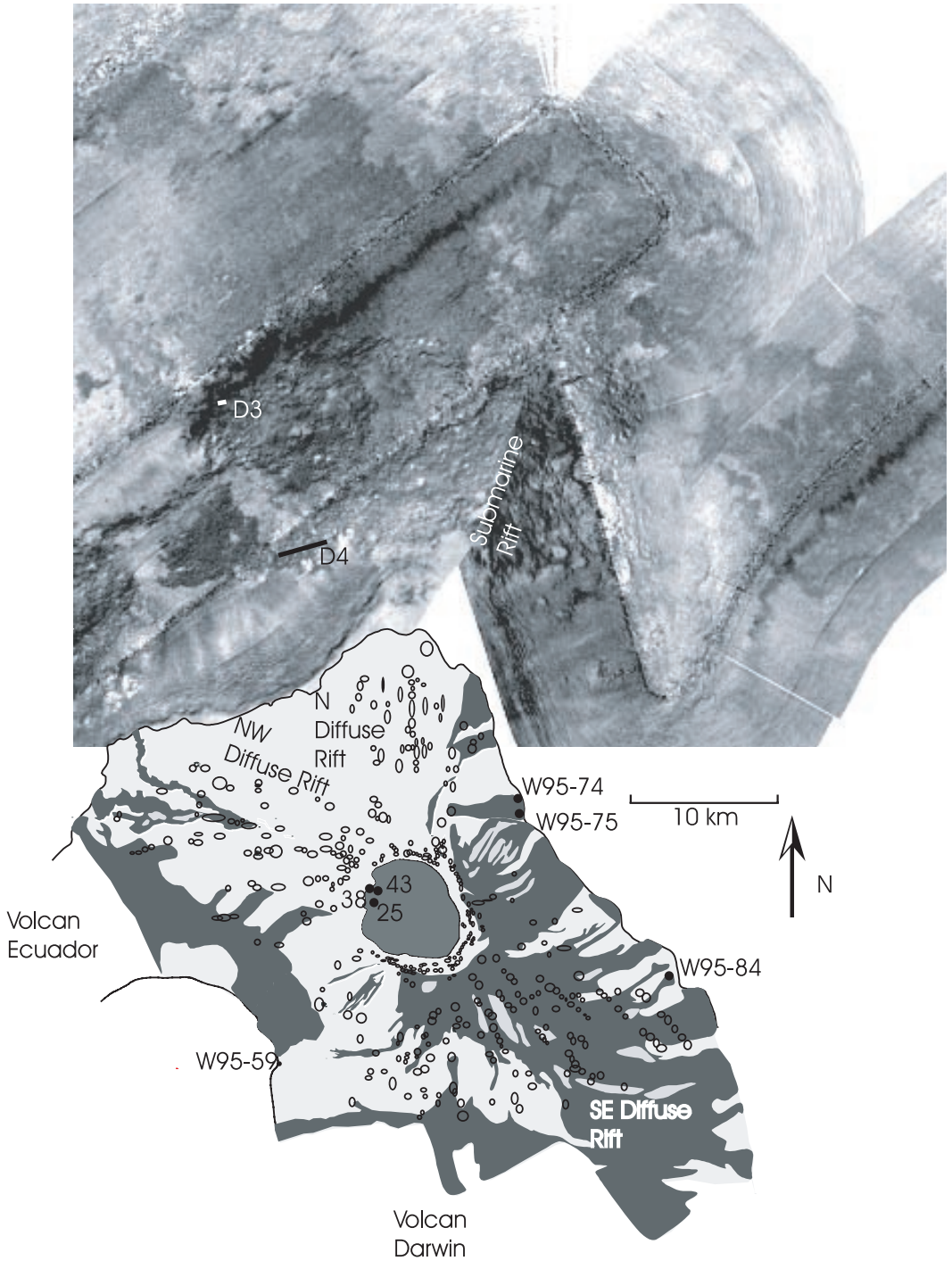

Fig. 3. Schematic geological map of Wolf volcano superimposed on side-scan sonar image of seafloor surrounding the volcano. On the side-scan sonar image, light color indicates a weak return signal. Location of the two dredges (D3, D4) on Wolf's submarine flanks are indicated. Grey shading indicates the distribution of young, unvegetated lava flows on the volcano flanks and in the caldera. Outlined circles and ellipses indicate volcanic vents. Locations of the samples for which age determinations have been made (Table 4) are shown.

Cerro Azul: Naumann & Geist, 2000; Sierra Negra: Reynolds *et al.*, 1995; Alcedo: Geist *et al.*, 1994), none of the dikes intrudes ring faults. A prominent graben cuts the southern summit plateau, parallel to the caldera wall and several hundred meters outboard of the caldera wall. Although many recent vents are located in this area, no fissures intrude the graben-forming faults. Consequently, we concur with Chadwick & Howard (1991), who noted

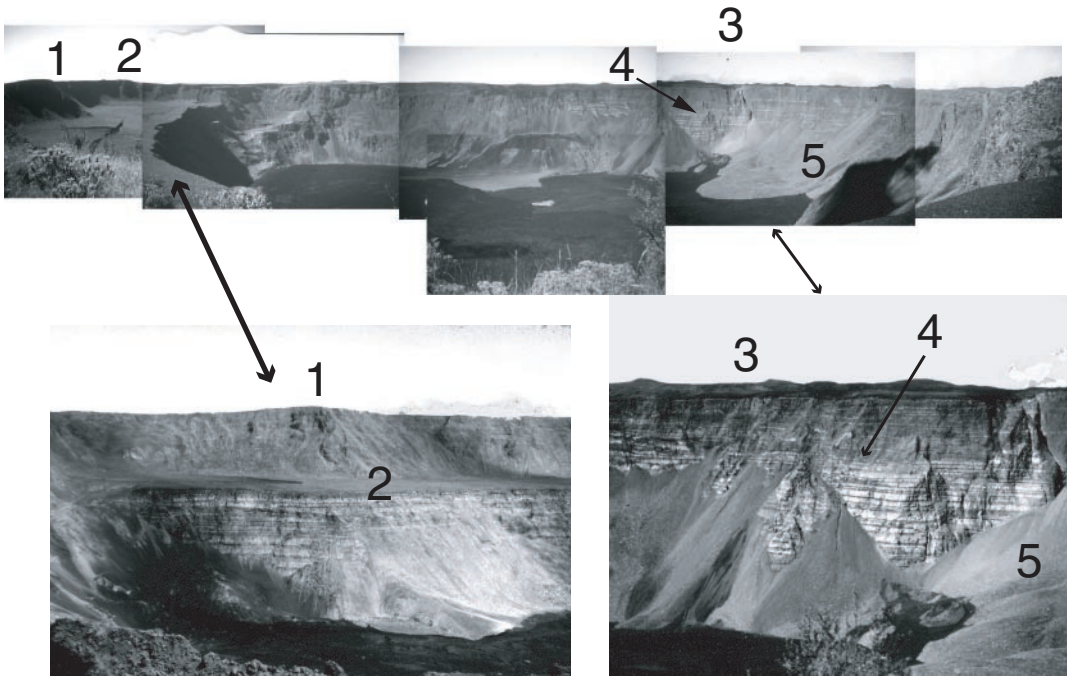

Fig. 4. (Top) Panorama of Wolf caldera, from the SW rim. The caldera is ~5 km across in this view and 700 m deep. Some of the features discussed in the text are as follows. 1, The highest point in the Galápagos Islands. The base of this rock rib exposes the oldest known rocks on Wolf volcano. 2, The bench, marking the level to which the caldera was filled. Young fissure cuts the bench. 3, Hills on the horizon mark locations of circumferential vents, some of which erupt lavas that then cascade down the caldera walls. 4, The best locality exposing the contact between caldera-filling facies and caldera rim facies. 5, The lobe of the largest avalanche deposit, which is overlain by young lava flow that has ponded in the caldera. (Bottom left) The bench, which is made up of caldera-filling lavas, as viewed from the SW caldera rim. The 1982 vent is visible in the lower left. (Bottom right) Detail of the contact between caldera-filling facies below, and caldera-rim facies above, on the south caldera wall.

that although the same stresses control the orientation of the caldera-forming faults and dike attitude, dikes rarely if ever intrude the caldera ring faults in Galápagos-type shield volcanoes.

InSAR data indicate that Wolf's caldera floor is actively inflating (Amelung *et al.*, 2000). Although the deformation measurements are one-dimensional and therefore do not constrain the geometry of the source strongly, the signal at Wolf is a symmetrical bull's eye confined to the caldera, characteristic of a spherical source or circular sill. Uplift of 14 mm/year between 1992 and 1998 is consistent with a modeled depth to the pressure source of 1·6 km (Amelung *et al.*, 2000), which we interpret to be the top of Wolf's magma chamber.

Stratigraphic designations and age determinations

We divide Wolf lava flows into five geological units. The stratigraphic order of the units within the caldera is constrained by the field relationships discussed above, and includes both superposition and facies interpretations. From youngest to oldest (excepting the flank lavas), the units are:

(1) historical lavas;
(2) Episode 2 rim facies lavas;
(3) caldera-filling lavas;
(4) Episode 1 rim facies lavas;
(5) flank lavas from diffuse rift zones.

Historical activity

Wolf volcano has experienced 10 witnessed eruptions since 1797, the most recent in 1982 (Simkin & Siebert, 1994). The 1982 eruption issued from vents both within the caldera (Fig. 4) and on the SE flank. The caldera floor eruption had particularly vigorous fire fountaining, which deposited over a meter of cinders on the caldera rim, 700 m higher than the vent. Records of the other historical eruptions indicate that much of the recent activity has been from the southern diffuse rift and the eastern circumferential rift; the distribution of vegetation on the volcano suggests this pattern has been consistent throughout the most recent phase of activity (Fig. 3).

Older activity: age constraints

The oldest lavas exposed on Wolf volcano for which we have stratigraphic control are the Episode 1 rim facies lavas that buttress the caldera-filling lavas of the western bench. Unfortunately, many of the older, lowermost flows are slightly propyllitically altered by dikes. The oldest visibly fresh lava (W95-43) yields an $^{39}Ar/^{40}Ar$

plateau age of 173 ± 20 ka and an isochron age of 71 ± 33 ka (Table 4). An overlying lava flow from the next stage of caldera growth has a plateau age of 20 ± 22 ka. Although these age determinations do not have much statistical significance, they suggest that the main episode of shield growth took place rapidly and was well under way by 100 ka and may be significantly younger.

Cosmogenic ^{3}He exposure dates (Kurz, 1986) of flank lavas range from <500 years to 1800 ± 800 years (five determinations total; Table 4). Cosmogenic ^{3}He in these samples is at or below the detection limit, because of the young ages and low production rates (at low elevations and low latitude); thus only upper age limits could be obtained. These age determinations are consistent with stratigraphic relationships, however. W95-75 and W95-84, which have exposure ages <500 years, are sparsely vegetated. The flow from which W95-74 was taken has an exposure age of <1000 years and underlies the W95-75 flow. Sample W95-59 comes from a visibly older vegetated flow and has an exposure age of 1800 ± 800 years. The age limits indicate that the large areas on the flanks of the volcano are resurfaced quickly, perhaps as often as every few thousand years. This is comparable with resurfacing rates at Sierra Negra (Reynolds *et al.*, 1995), Cerro Azul (Naumann & Geist, 2000), and Fernandina volcanoes (Kurz & Geist, 1999; M. Kurz, unpublished data, 2005).

A sample taken from the part of the caldera wall exposing the caldera-filling bench lavas yielded a ^{3}He exposure age of <200 years (W95-25). The age was calculated by taking horizon measurements from the sample location, and using the proportion of the visible sky to scale the sample's exposure to cosmic rays. This section of the wall may have been exposed by recent mass-wasting, and the calculated age only brackets the minimum age of the most recent caldera collapse.

PETROLOGY AND GEOCHEMISTRY OF WOLF'S LAVAS

The most notable attribute of Wolf's lavas is their overall depleted Sr–Nd–Pb–He isotopic compositions, which are comparable to MORB from the Galápagos spreading center sampled over 400 km from the Galápagos Islands (Fig. 5; Schilling *et al.*, 2003). Wolf lavas have the most depleted Sr, Nd, and Pb isotopic ratios in the western Galápagos, with only Darwin Volcano having similar isotopic compositions. All of the other western volcanoes, including the neighboring volcanoes Ecuador and Roca Redonda, have Sr and Nd isotopic compositions much closer to the average 'PLUME' component, as defined by Harpp & White (2001).

Another important aspect of the Wolf suite is its remarkable homogeneity: all of the aphyric lavas have 5 < MgO < 6·5 wt % and small ranges in incompatible trace element ratios. This geochemical monotony is characteristic of several of the most active western Galápagos shields, including Sierra Negra (Reynolds & Geist, 1995) and Fernandina (Allan & Simkin, 2000). It is unlike Cerro Azul (Naumann *et al.*, 2002), Roca Redonda (Standish *et al.*, 1998), and Volcan Ecuador (Geist *et al.*, 2002), which have also erupted high-Mg basalts, including picrites, and Alcedo Volcano, which has erupted a basalt-to-rhyolite sequence (Geist *et al.*, 1994). Sufficient evidence now supports the classification of the western shields as either 'monotonous' or 'diverse' petrological types (Geist & Teasdale, 2001), and Wolf's lava flows are of the 'monotonous' type.

Isotopic variations

The new results for Sr, Nd, and Pb isotope data correspond closely to those reported for three reconnaissance samples by White *et al.* (1993). With the exception of a single illegitimate magma that erupted low on the SW flank of the volcano (W95-61; a lava that probably intruded into the Wolf edifice from Fernandina or Ecuador volcano and will not be considered further; Geist *et al.*, 1999), Wolf's lavas display a limited range of isotopic compositions, with ε_{Nd} ranging from only +7·5 to +8·7 (Fig. 5).

Comparison of the isotopic composition of Wolf volcano lavas with those of GSC lavas is problematic, owing to the exceptional compositional diversity of the GSC (e.g. Schilling *et al.*, 2003). Sr, Nd, Pb, and Hf isotopic ratios of lavas from the GSC decrease linearly away from the area of peak influence of the Galápagos hotspot at 91°W, which has been interpreted as resulting from interaction between the Galápagos plume and normal MORB source (e.g. Schilling *et al.*, 2003). Our approach in comparing the compositions of Wolf volcano lavas with those of the GSC is to select the subset of GSC samples where the Nd isotopic ratio gradient intersects the range of Nd isotopic compositions found at Wolf volcano, which occurs at longitudes 94·1–94·7°W and 89·1–89·7°W along the GSC (Table 5). This comparison shows that, with the exception of slightly lower ^{208}Pb/^{204}Pb at Wolf (Fig. 5 and Table 5), the Sr, Pb, and Hf isotopic ratios of Wolf volcano lavas are the same as those measured for GSC samples at 94·1–94·7°W and 89·1–89·7°W. These GSC samples are 250–410 km away, along axis, from the peak influence of the Galápagos hotspot (Schilling *et al.*, 2003). Hf isotopic ratios of Wolf lavas are also the same as those from the GSC from those areas (see Blichert-Toft & White, 2003; Schilling *et al.*, 2003), as are ratios of highly incompatible elements (Table 5).

Helium isotopes are the major exception to the correspondence between Wolf volcano isotopic compositions and those from the GSC at 94·1–94·7°W and 89·1–89·7°W. Wolf ^{3}He/^{4}He values, which range from 8·6 to

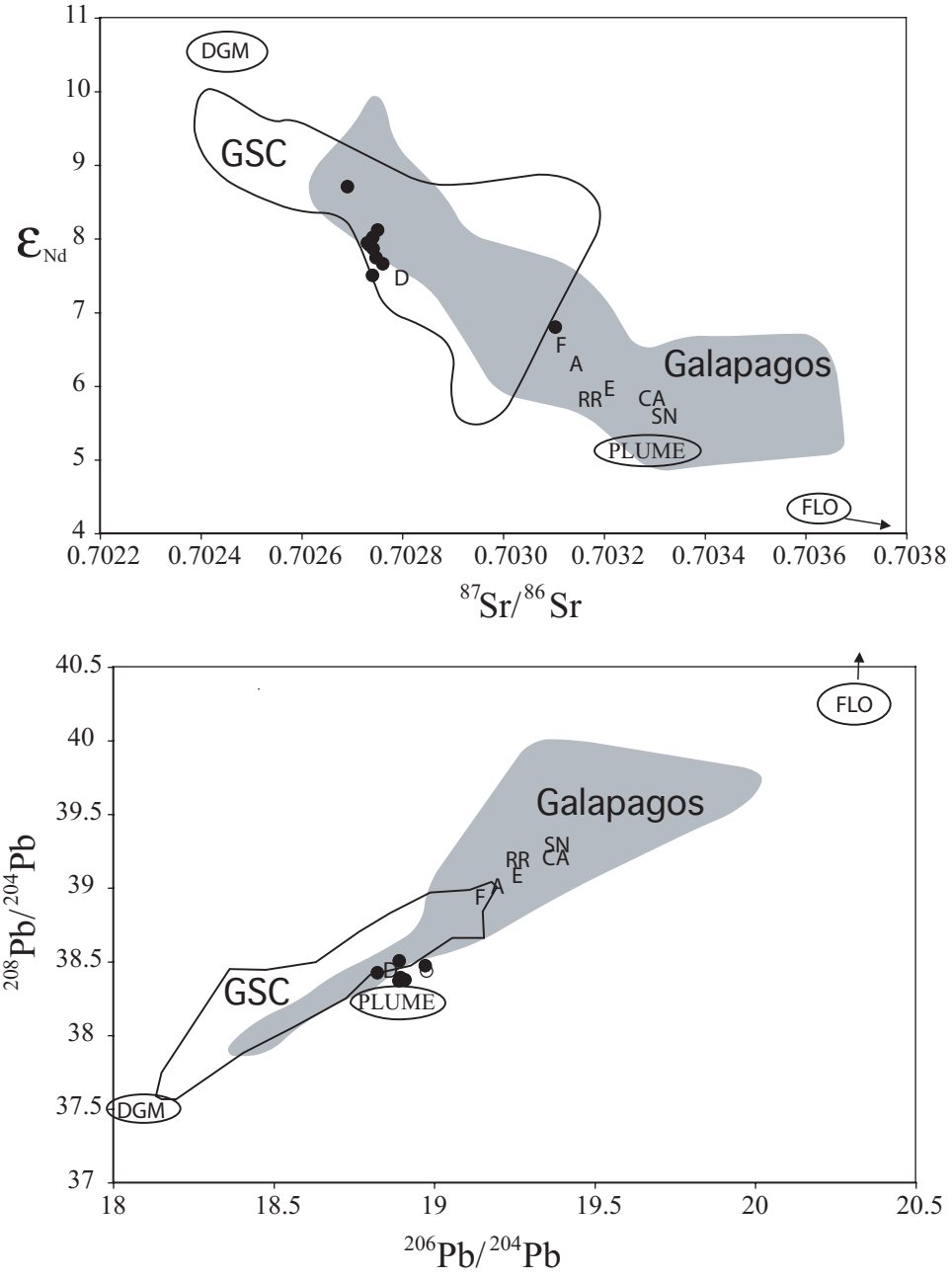

Fig. 5. Sr–Nd–Pb isotopic composition of lavas from Wolf volcano (●), compared with the range for the GSC (Schilling *et al.*, 2003) and the entire Galápagos Archipelago (White *et al.* 1993). Wolf data are those reported in Table 3 and three samples from White *et al.* (1993); average values are used for samples that were analyzed at both Cornell and WHOI. Mantle source reservoirs assigned by Harpp & White (2001) are DGM, PLUME, and FLO. Average values for the other western Galápagos volcanoes (from White *et al.*, 1993) are indicated by letters (E, Ecuador; F, Fernandina; RR, Roca Redonda; D, Darwin; A, Alcedo; SN, Sierra Negra; CA, Cerro Azul).

9·8 R_a, overlap with 'normal MORB' (e.g. Kurz & Jenkins, 1981) but are elevated with respect to the GSC (5·9–8·5 Ra; Detrick *et al.*, 2002; D. Graham, personal communication, 2004).

A search of the GEOROC ocean island database (http://georoc.mpch-mainz.gwdg.de/) indicates that Wolf volcano is the most MORB-like active intraplate volcano in the world, in terms of its Sr and Nd isotope composition. Genovesa volcano in the northeastern Galápagos, which is not known to be historically active, has even more depleted isotopic compositions (White *et al.*, 1993; Harpp *et al.*, 2002). Harpp *et al.* (2002) have

Table 5: Comparison between isotopic and trace element compositions of Wolf lavas and GSC lavas from 94·1° to 94·7° W and from 89·1° to 89·7° W

	$^{143}Nd/^{144}Nd$	$^{87}Sr/^{86}Sr$	$^{206}Pb/^{204}Pb$	$^{207}Pb/^{204}Pb$	$^{208}Pb/^{204}Pb$	$^{3}He/^{4}He\ R_a$	La/Nb	Ba/Nb	$^{176}Hf/^{177}Hf$
GSC range	0·512995–	0·70273–	18·69–	15·54–	38·47–	5·9–8·4	0·6–1·1	4·8–6·0	0·283087–
	0·513048	0·70291	19·06	15·60	38·72				0·283148
Wolf average	0·513031	0·70277	18·91	15·55	38·42	9·0	1·0 ± 0·3	5·2 ± 0·8	0·283130

Data from Detrick *et al.* (2002), Schilling *et al.* (2003), and D. Graham (personal communication, 2004).

shown that Genovesa contains insignificant amounts of plume material and exists because of the shallow base level of the seafloor near the spreading ridge and high heat flow owing to the proximity of the Galápagos plume to the GSC. With Wolf volcano, the observation of a depleted source is especially important, because it is distinctly related to the plume province and is no different from any other of the Galápagos shields in its morphology and eruptive history. This begs the question: how can a hotspot volcano have such small amounts of plume material?

Petrography and elemental variations

Most Wolf lavas contain phenocrysts and microphenocrysts of plagioclase, augite, and sparse olivine. The plagioclase-phyric rocks have between <1 and 23% phenocrysts up to 6 mm long. Few of the rim-facies lava we inspected (roughly 100 flows) are strongly (>5%) plagioclase-phyric, whereas the majority of caldera-filling and flank flows are strongly plagioclase-phyric. Plagioclase phenocrysts tend to be irregularly zoned, with three types of zoning patterns (Fig. 6). The most common zoning pattern is one where the core has irregular variations of about 4–10 mol % An over short (tens of microns) distances. Other grains have cores with essentially constant composition (<2% An change). A few of the microphenocrysts have steady normal zoning. There is no apparent relationship between the composition of the whole rock and the compositions of cores or rims of plagioclase grains contained within those rocks.

Olivine phenocrysts are sparse in Wolf lavas. Microprobe analyses of olivines in two lavas (Mg-number = 50·6 and 51·7) that contain phenocrysts reveal that most grains are normally zoned, with cores of about $Fo_{82–89}$ and rims of $Fo_{78–83}$. Clinopyroxene phenocrysts occur in many of the lavas in abundances of a few percent, especially the plagioclase-phyric lavas. The analyzed crystals have Mg-number ranging from 75 to 83 and most Al_2O_3 concentrations ranging from 3 to 4%.

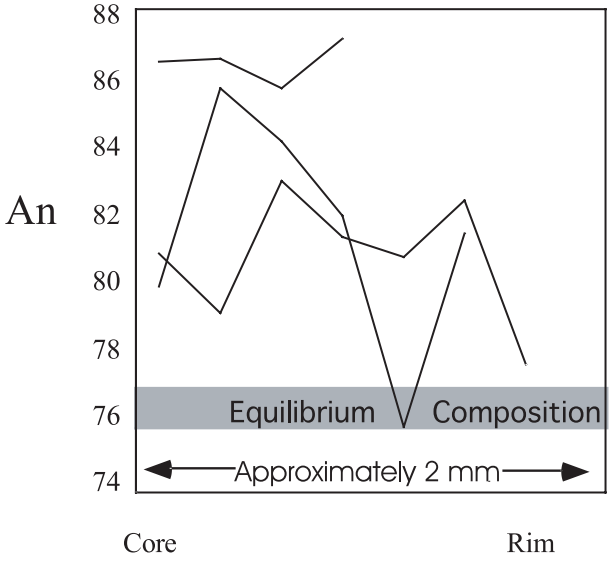

Fig. 6. Zoning profiles across plagioclase grains in sample W95-72, which is a plagioclase-accumulative lava. Plagioclase in equilibrium with a melt with equivalent Mg-number is An_{76} (as calculated by MELTS, Ghiorso & Sack, 1995).

Two aspects of the whole-rock geochemistry stand out (Tables 1 and 2): the small range in Mg-number of almost all Wolf lavas, and the high Al_2O_3 concentrations of some of the lavas (Fig. 7). All aphyric lavas and the submarine glasses lie within a narrow band in terms of Al_2O_3 and Mg-number variations (Fig. 7), but the plagioclase-phyric flows are much richer in Al_2O_3. With the exception of the plagioclase-phyric rocks, there is a small range in MgO; all but a few have between 6·5 and 5·5% MgO. The limited range in MgO is matched by even less variation in ratios between incompatible trace elements. For example, if the illegitimate lava W95-61 is not considered, the relative standard deviation (RSD) of Nb/Zr is 6%, only twice the propagated analytical uncertainty. Ratios of La/Sm for the nine measured samples, which were chosen to reflect the entire range of compositions, have an RSD of only

4%, again barely beyond propagated analytical uncertainty. Otherwise, the Wolf suite displays trends typical of other Galápagos volcanoes whose magmas have evolved by low- to medium-pressure fractional crystallization, with increasing alkalis, FeO, and incompatible elements with decreasing Mg-number. Variations in CaO/Al_2O_3 ratios, which are an effective diagnostic feature of the fractionating assemblage, correlate well with Mg-number, indicating some clinopyroxene control (Fig. 7). Sr/Y, a measure of plagioclase fractionation, correlates with Sc/Y, an indicator of clinopyroxene fractionation (Fig. 8).

Despite the depleted isotopic compositions of Wolf's lava, REEs exhibit relatively light REE (LREE)-enriched patterns unlike MORB (Fig. 9) The REE patterns are nearly flat from La to Nd, then have steep negative slopes. Small negative or positive europium anomalies are apparent in most lavas, and Eu* correlates well with Al_2O_3 concentration.

Temporal variations

The mapping and stratigraphic assignments permit an assessment of variations in Wolf's magma composition with time. The analysis of temporal variation utilizes a subset of the analyses that includes only samples whose relative stratigraphic position is confidently known, mostly from the caldera walls (Fig. 10). Magma temperature and the extent of differentiation, as indicated by bulk-rock MgO content, show no systematic trend with time. Al_2O_3, a measure of the amount of plagioclase phenocrysts in the rock, also exhibits no systematic trends with time; Al_2O_3-rich lavas are sporadically present throughout the stratigraphic section. Incompatible trace element ratios also do not form a discernible trend with time, and much of the range of Nb/Zr is represented by lavas erupted over the past 500 years (Fig. 10). The compositions of lava erupted during caldera-filling and caldera collapse cycles are

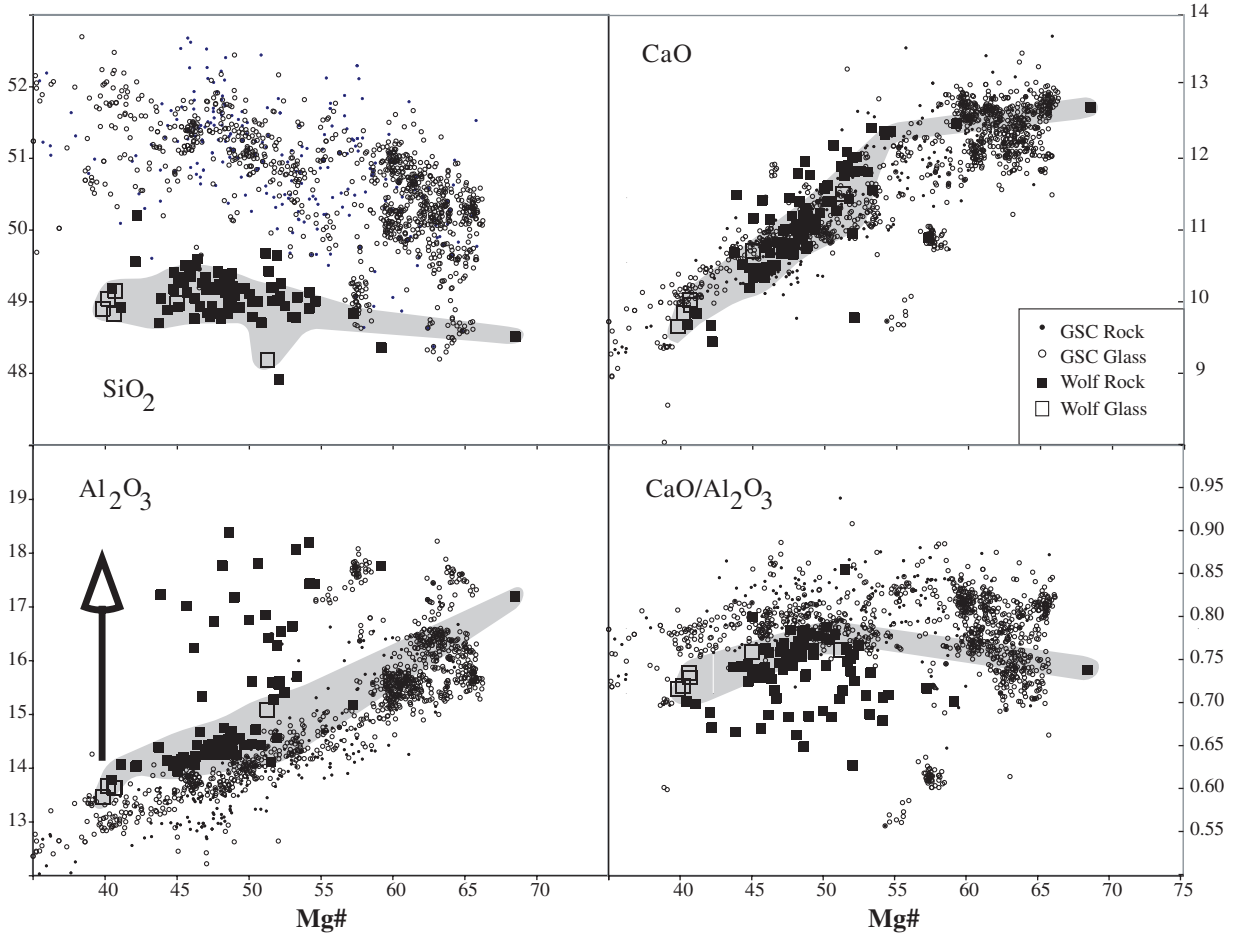

Fig. 7. Major element variation of Wolf lavas compared with those from the GSC (complete dataset of GSC rocks and glasses compiled from PETDB database at http://www.petdb.org/). Field of non-accumulative Wolf lavas (those with <5% plagioclase phenocrysts) is shown in gray. Arrow on Al_2O_3 diagram indicates the compositional effect of adding 20% plagioclase.

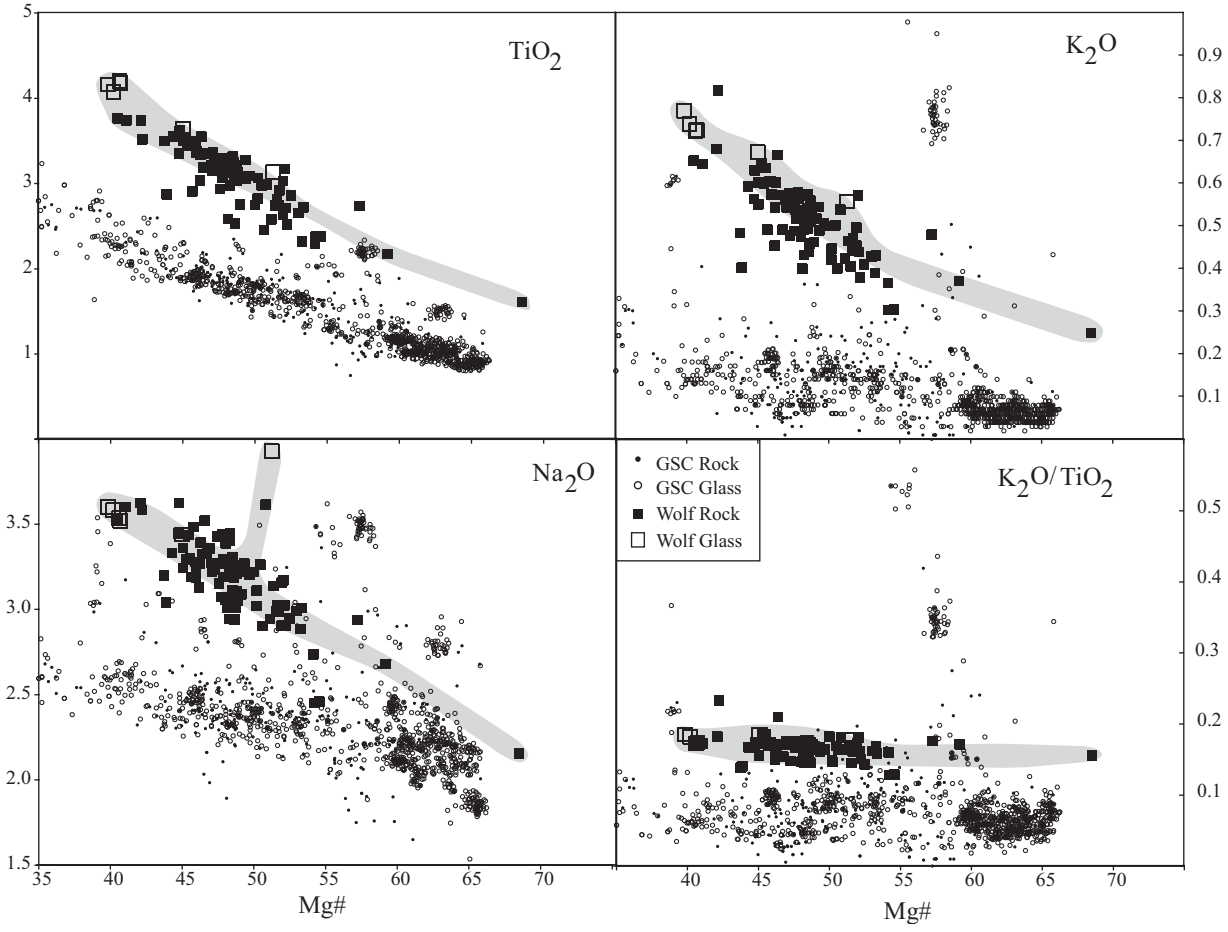

Fig. 7. Continued.

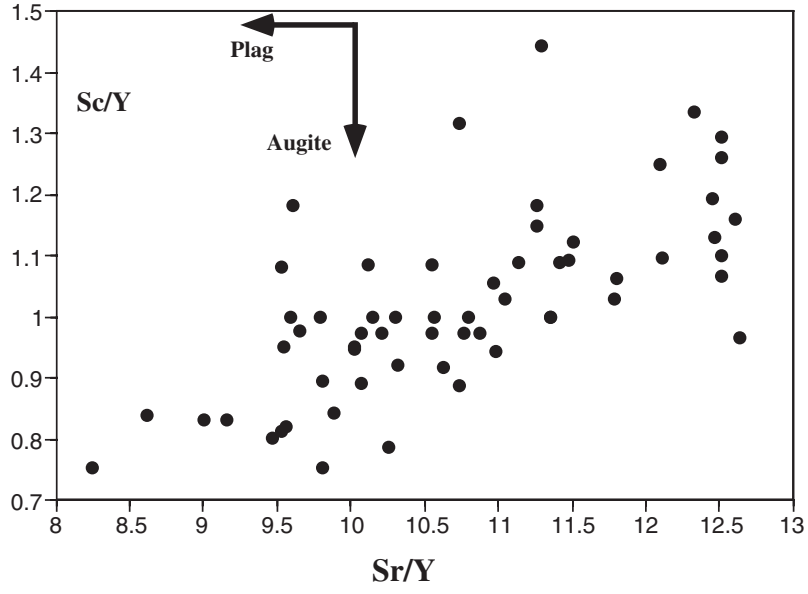

Fig. 8. Sc/Y and Sr/Y distributions in Wolf lavas. The data are explained by cotectic crystallization of clinopyroxene and plagioclase.

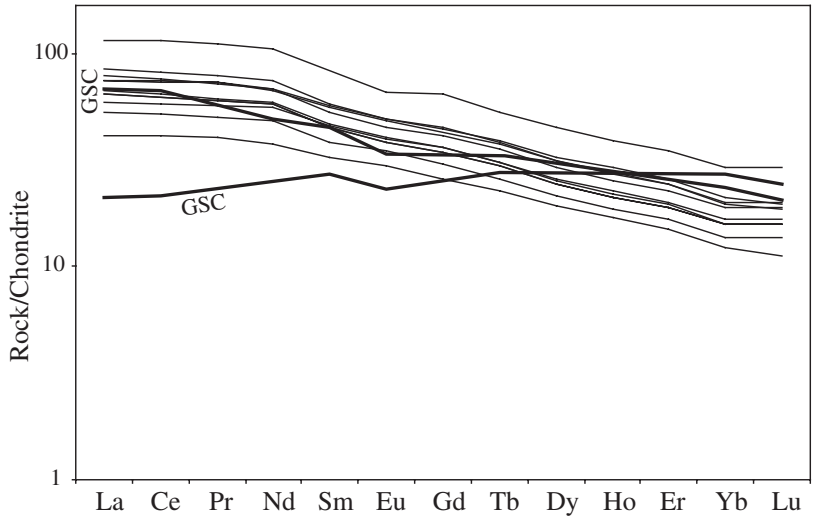

Fig. 9. Rare earth element compositions of Wolf lavas, compared with two samples of MORB from the GSC from regions with identical Nd-isotopic compositions at 94·1–94·7°W and 89·1–89·7°W [data from Schilling *et al.* (1982)].

indistinguishable from each other, as are submarine compared with subaerial lavas.

DISCUSSION

Volcanic development of Wolf volcano

The caldera at Wolf volcano has undergone at least two major phases of collapse, punctuated by an episode of caldera filling. Because the bottom of the first phase of rim facies lavas is unexposed, the depth of the initial caldera is not known, but it was at least as deep as the present caldera (700 m). The caldera-filling stage involved the accumulation of $>35\ km^3$ of lava. Then, the caldera collapsed by at least 450 m (the height of the stranded bench), although it is unclear whether this occurred incrementally or in a single event. It is possible that the caldera is in a renewed caldera-filling phase, because the 1982 eruption produced a voluminous ponded a'a' flow but was not accompanied by caldera collapse.

At least three possibilities exist for the transition between caldera-filling and caldera-collapse modes. First, caldera filling may occur when the flux of magma from below increases. Filling takes place when the rate of magma supply to the uppermost magma reservoir exceeds the eruptive rate. Collapse is the result of eruption rates higher than input rates. If caldera filling resulted from increased magma supply, then one would expect to see more primitive magmas in the caldera-filling stage, clearly not the case at Wolf (Fig. 10). Second, caldera collapse could be the result of increased amounts of magma erupting from the flanks of the volcano, whereas caldera filling could be stages when most magma erupts at the summit. Without better exposure and age determinations of the flank lavas, and perhaps a deep drill hole, this is a difficult hypothesis to test. Third, the caldera collapse may not relate simply to the emptying of the shallow magma reservoir. Instead, it could largely be the result of gravitational compensation of high-density cumulates beneath the summit (Walker, 1988).

Mapping of Wolf confirms some previous interpretations of the development of Galápagos shield morphology (Geist *et al.*, 1994; Reynolds *et al.*, 1995; Naumann & Geist, 2000). Most flank eruptions on Wolf are from diffuse rift zones. Outward-directed tension caused by the steep eastern and western slopes tends to repel outward-directed dikes from those sectors (Naumann & Geist, 2000), and loading of adjacent Darwin and Roca Redonda volcanoes directs dikes to the north and SE. Eruption from radial vents is self-perpetuating; satellite vents build topography, which buttresses the summit carapace, and causes further eruption in that sector of the volcano (Fiske & Jackson, 1972).

The steep eastern and western flanks could be interpreted as landslide headwalls, because they form concave shorelines, and there is a steep, 3 km slope to abyssal depths east of Wolf. If either flank has been involved in a landslide, all evidence of it has been buried by younger flows, and there is no suggestion of mass-wasting deposits in side-scan images of the adjacent seafloor (Fig. 3 and Kurz *et al.*, 2001).

Mouginis-Mark *et al.* (1996) showed that steep flanks on Galápagos-type shields are not simply due to building the summit carapace by eruptions from circumferential fractures along the caldera rim (Simkin, 1972). Instead, the summit builds up symmetrically from eruptions from circumferential summit vents, but the growth of flanks

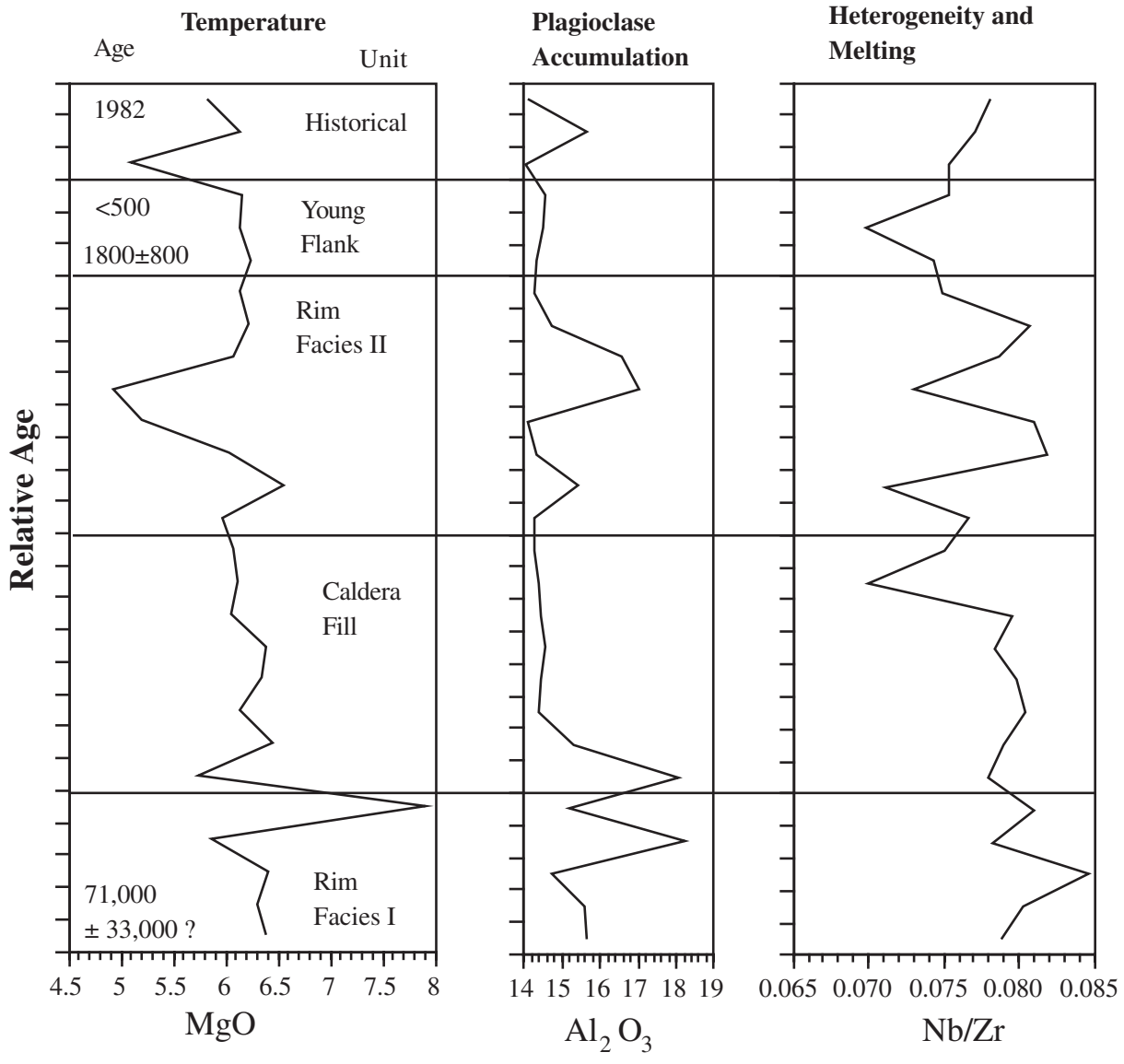

Fig. 10. Stratigraphic variation of MgO (wt %), Al_2O_3 (wt %), and Nb/Zr, based only on those samples whose relative position is known. Boundaries between the units are indicated by horizontal lines, and could represent major breaks in time. Stratigraphic position of samples with age determinations (Table 4) is shown.

in some sectors does not keep up with the summit construction rate. Steep profiles caused by the paucity of satellite vents on the lower flanks also explain the SW face of Cerro Azul (Naumann & Geist, 2000), the north and west faces of Fernandina (Rowland & Munro, 1992), and oceanic volcanoes worldwide (Rowland & Garbeil, 2000).

Petrological evolution of Wolf magmas

Evidence for plagioclase accumulation

The large quantities of plagioclase phenocrysts in Wolf lavas could be the result of either crystallization from liquids with large amounts of Al_2O_3 or accumulation of plagioclase in basaltic liquid with 'normal' concentrations of Al_2O_3. Several lines of evidence point to accumulation as the dominant process. First, most whole-rock analyses of subaerial rocks have distinctly higher Al_2O_3 concentrations than submarine glasses and aphyric lavas, none of which have $Al_2O_3 > 15\%$ (Fig. 7). Second, the trend on the Al_2O_3 vs MgO diagram (Fig. 7) is consistent with plagioclase + augite + olivine removal from the aphyric magmas along a single liquid line of descent, and up to 20% plagioclase accumulation in the high-alumina lavas ($Al_2O_3 > 15\%$). Third, plagioclase zonation patterns (Fig. 6) indicate that individual plagioclase crystals grew

from a number of liquids; the large jumps in composition are unlike those that develop from diffusion-controlled growth from a single static liquid (Pearce & Kolisnik, 1990). Fourth, rocks with Al_2O_3 >15% have anomalously high Sr and Eu contents (Tables 1 and 2). We conclude that Wolf lavas with >15% Al_2O_3 have accumulated plagioclase and do not represent liquid compositions. As with Fernandina (Allan & Simkin, 2000), Sierra Negra (Reynolds & Geist, 1995), Alcedo (Geist *et al.*, 1994), and Ecuador (Geist *et al.*, 2002), plagioclase accumulation is a major petrogenetic process at Wolf.

Evidence for fractional crystallization

Mass balance and thermodynamic calculations indicate that most of the compositional variation among the non-accumulative lavas can be explained by ~46% fractional crystallization of olivine + plagioclase + clinopyroxene, in proportions of approximately 1:11:11 (calculated by least-squares mass balance and application of MELTS; Ghiorso & Sack, 1995). The MELTS models indicate that this compositional range corresponds to cooling of about 60°C. In fact, the majority of the lavas have between 6·6 and 5·3% MgO, corresponding to a temperature of 1150 ± 11°C. The relatively constant incompatible trace element and isotopic ratios indicate fractionation from similar parental magmas.

Depth of storage

MELTS calculations (Ghiorso & Sack, 1995) indicate that the magmas are saturated with plagioclase + olivine + clinopyroxene only at $P < 2$ kbar, and projections using the technique of Grove *et al.* (1992) yield pressures of 1–3 kbar (Geist *et al.*, 1998). Thus, most, if not all, of Wolf's magmas last equilibrated at very shallow depths, which is consistent with the deformation modeling of Amelung *et al.* (2000), which indicates that the top of Wolf's magma chamber is only 1·6 km beneath the caldera floor (~700 m below sea level).

A model for Wolf's magma chamber

The volume of Wolf's magma chamber can be estimated using the technique proposed by Albarède (1993), which postulates that the magma reservoir dampens the compositional variability of intruded magmas. Historically erupted lava and flows whose ages are constrained by exposure dating show an increase in Nb/Zr over the past 500 years (Fig. 10). If extreme values of Nb/Zr in Wolf magma are used to estimate the possible range of compositions of the infilling magma, then a residence time of 3–18 kyr results. To estimate the eruption rate, we assume that growth is greatest at the summit of the volcano and tapers to nil at the coastline (after Naumann & Geist, 2000). Although the ages of the lavas remain uncertain, we assume that the upper 330 m of the summit carapace was emplaced in the past 70–170 kyr, as suggested by the argon ages. With these values, eruption rates ranging from approximately $0{\cdot}4 \times 10^6$ to $1{\cdot}0 \times 10^6$ m^3/year are calculated. This range of residence time and eruptive rate estimates results in a chamber volume of 1·2–18 km^3. If the chamber has the diameter of the caldera, then it is only between 50 and 800 m thick.

We propose a model for Wolf's magmatic plumbing system that is motivated by the work of Sinton & Detrick (1992) on magma chambers beneath fast spreading mid-ocean ridges. They show that a thin melt lens overlies a thick column of gabbroic mush. Mush is defined as magma having between 50 and 75% crystals, which, owing to its high effective viscosity, cannot erupt (Marsh, 1981). The mush column is surrounded on its sides by magma of even higher crystallinity that behaves plastically. Repeated intrusion of hot magma keeps the mush well above its solidus and prevents further chemical differentiation. The principal difference between the Sinton & Detrick (1992) model and the one proposed here is that at a Galápagos shield, the cumulate mush is not carried away by seafloor spreading. Instead, the intrusive volume is accommodated by crustal thickening.

Our model for the Wolf magma chamber, and for Galápagos magma chambers in general (Geist & Teasdale, 2001), is that the uppermost magma body beneath Wolf volcano is a thin (<800 m thick) sill that lies at <2 km depth (Fig. 11). Crystallization of plagioclase + clinopyroxene + olivine takes place during ascent and within the sill, and plagioclase accumulates at the roof of the sill, whereas the mafic minerals (plus some plagioclase) are deposited on the floor, making a cumulate mush of wehrlite and olivine gabbro. Plagioclase flotation is consistent with calculated densities of aphyric liquids of 2·72 g/cm^3 (Lange & Carmichael, 1990), relative to plagioclase of the appropriate composition with a density of 2·64 g/cm^3. Positive gravity anomalies of ~30 mgal at Fernandina (Ryland, 1971) and Sierra Negra (D. Johnson, personal communication, 2004) provide further evidence for the accumulation of dense cumulates beneath these calderas. The magma body is effectively in a thermochemical steady state, where the intrusion of hot magma balances the heat flow out of the body, buffering the system to ~1150°C in the case of Wolf Volcano. An additional factor in maintaining thermal and compositional buffering is reaction of ascending magmas with the cumulate mush (e.g. Bedard, 1993; Albarède *et al.*, 1997). Primitive magmas that are undersaturated with plagioclase, olivine, or clinopyroxene react with those minerals in the mush column, and, owing to their high enthalpies of fusion, quickly cool the magma to the steady-state temperature and force multiple saturation. Another ramification of this model is that few of the crystals carried by a silicate liquid actually crystallized

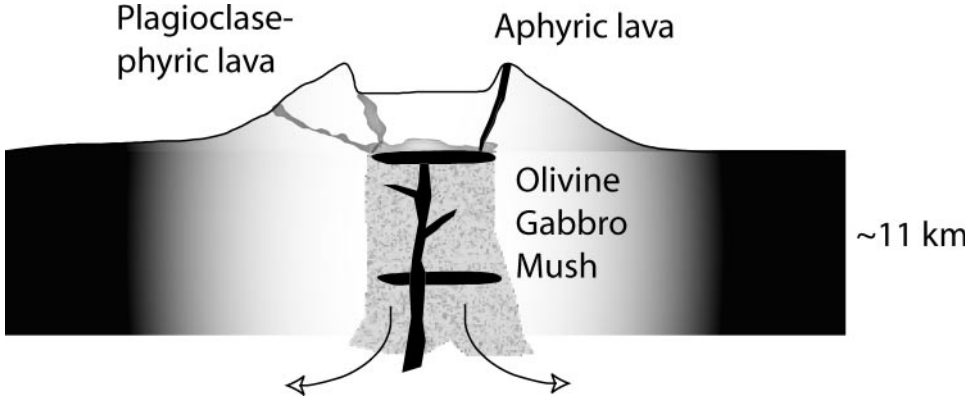

Fig. 11. Conceptual model of the Wolf magmatic plumbing system. Hot magma reacts with olivine gabbro mush, buffering temperature and composition. The last stage of evolution is in a shallow sill, where plagioclase floats, and olivine, augite, and plagioclase are deposited on the floor. Plagioclase-phyric magmas rarely erupt from summit vents but are common on the flanks and caldera floor.

from it, as is apparent by the plagioclase compositions (Fig. 6).

Melting at the margins of a plume

It has been proposed that the depleted mantle source end-member of the Galápagos region is also part of the Galápagos plume (Hoernle *et al.*, 2000), as has also been proposed for Iceland (although this remains a contentious issue; see Hanan *et al.*, 2000; Fitton *et al.*, 2003). The hypothesis that the depleted component is part of the Iceland plume was motivated by the observation that some isotopically depleted lavas there have lower Nb/Zr ratios than MORB from the North Atlantic (Hardarson & Fitton, 1997). Wolf lacks any lavas with Nb/Zr ratios as low as those of the GSC, thus Nb–Zr–Y trends do not help diagnose the depleted source in the Galápagos archipelago. As Table 5 and Fig. 5 show, Wolf lavas have nearly identical Nd, Sr, Pb, and Hf isotopic ratios, as well as Ba/Nb and La/Nb ratios, to those from GSC at 94·1–94·7°W and 89·1–89·7°W. $^{3}He/^{4}He$ ratios are significantly higher in Wolf lavas than those of the GSC, however. The different behavior of helium in relation to the other radiogenic isotopes within the Galápagos archipelago was recognized by Graham *et al.* (1993) and Kurz & Geist (1999). The latter workers attributed this to preferential removal of helium by low degrees of partial melting (and extreme incompatibility) as the plume ascends, which removes most of the helium, but not the Sr, Nd, Hf, and Pb, from the plume material before it mixes with the shallow mantle. Because Wolf volcano and parts of the GSC far removed from the archipelago have identical isotopic and trace element ratios (with the exception of helium and very slightly different $^{206}Pb/^{204}Pb$), we conclude that the depleted isotopic composition of Wolf magmas originates from the upper mantle.

Calculation of the amount of plume- and depleted-mantle-contributed Sr, Nd, and Pb is problematic, because the Galápagos plume has been demonstrated to be isotopically heterogeneous (e.g. Geist *et al.*, 1988; White *et al.*, 1993; Kurz & Geist, 1999; Hoernle *et al.*, 2000; Harpp & White, 2001). If the isotopic compositions of the depleted ('DGM') and 'PLUME' end-members designated by Harpp & White (2001) are used, then 60% of the Sr and 55% of the Nd in Wolf magma come from the depleted mantle (Fig. 5); however, none of the Pb could come from the Harpp & White (2001) depleted source, as Wolf lavas have Pb isotopic ratios that are equivalent to their 'PLUME' reservoir. If their 'FLO' source is used (FLO being part of the plume that is preferentially sampled at Floreana volcano), then 84% of the Sr, 63% of the Nd, and 71–76% of the Pb is from the depleted mantle.

Wolf's magmas differ significantly in trace and major element composition from GSC magmas, however (Figs 7, 9, and 12). The most important of these differences are: (1) Wolf magmas are richer in all of the incompatible elements (e.g. K, Ti, P, and Na; Fig. 7); (2) Wolf magmas have higher La/Yb and Tb/Yb ratios (Fig. 12); (3) Wolf magmas are poorer in SiO_2 and FeO and richer in Al_2O_3 (Fig. 7).

The elevated incompatible trace element concentrations are best explained by lower degrees of partial melting at Wolf volcano compared with the GSC, both of which are dominated by the depleted mantle component but have a significant contribution of plume component. The absolute difference is impossible to assess, because even the most primitive lavas from both Wolf and the GSC have undergone extensive fractional crystallization of several phases, thus the primary magma's composition cannot be calculated by adding equilibrium olivine. A typical GSC lava with 7% MgO and similar isotopic compositions to those of Wolf lavas contains ~0·12%

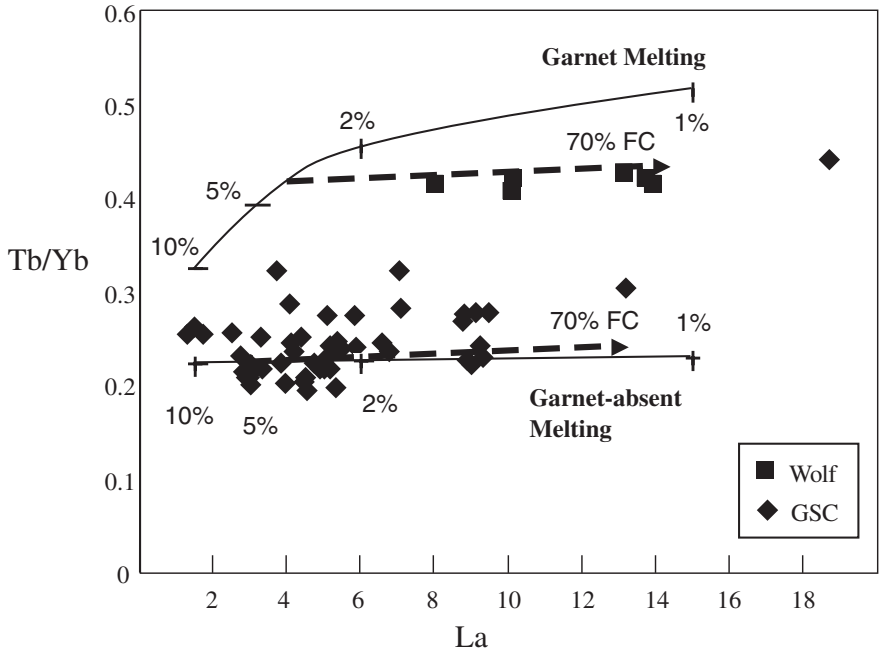

Fig. 12. Tb/Yb vs La illustrating HREE fractionation differences between Wolf volcano and GSC lavas. GSC magmas are modeled as batch modal partial melts of a lherzolite source with 20% clinopyroxene and 30% orthopyroxene. The Wolf magmas are effectively modeled by lower extents of partial melting of the same source, but with 5% garnet. Tick marks are at 1%, 2%, 5%, and 10% melting. Dashed subhorizontal arrows indicate the effects of 70% fractional crystallization (FC). Distribution coefficients are those of McKenzie & O'Nions (1991).

K_2O, whereas a typical Wolf magma with 7% MgO contains 0·33% K_2O. If the two magmas have undergone similar extents of fractionation to reach 7% MgO, the GSC MORB is the result of 10% partial melting, and K is considered to be perfectly incompatible, then the Wolf magma can be modeled as a 3·6% partial melt of the same MORB source. This calculation can be repeated for all of the incompatible trace elements, with similar results (Fig. 12).

The heavy REE (HREE) fractionation is probably caused by a greater role played by garnet in the source of Wolf's magmas. The difference between the REE patterns of Wolf and GSC magmas, as quantified by Tb/Yb ratios, can be well modeled by inclusion of 5% garnet in the Wolf source and its absence in that of the GSC (Fig. 12). Although MORBs may be partly derived in the presence of garnet, their trace element budget is controlled by melting in the spinel facies (e.g. Hirschmann & Stolper, 1996). Because the isotopic compositions of Wolf and GSC magmas overlap, the stronger garnet signal is probably not the result of different source compositions. In particular, $^{176}Hf/^{177}Hf$ ratios, which should be more radiogenic in rocks that have experienced ancient fractionation in the presence of garnet, are virtually the same in Wolf volcano, GSC, and EPR lavas (Table 5; see Blichert-Toft & White, 2001; Schilling *et al.*, 2003). Instead, enhanced fractionation of the trace elements by garnet is more probably the result of Wolf's magmas being generated at greater depths than GSC magmas, but from similar source compositions.

Lower extents of partial melting and deeper melt extraction are also consistent with the higher Al_2O_3 and lower SiO_2 contents of Wolf magmas (e.g. Asimow *et al.*, 2001; Ghiorso *et al.*, 2002). The systematically lower FeO concentrations in Wolf lavas compared with GSC compositions are probably the result of lower extents of melting as well. FeO concentrations in primary magmas increase as the extent of melting increases and with increasing pressure (e.g. Asimow *et al.*, 2001). In the case of Wolf, the degree of melting effects must overwhelm the pressure differences.

It has been proposed that Wolf and all of the volcanoes in the Galápagos with a depleted isotopic signature are the result of entrainment of upper mantle into the Galápagos plume by toroidal mixing into the core of the plume (Geist *et al.*, 1988; White *et al.*, 1993; Harpp & White, 2001). That hypothesis has several problems with respect to Wolf volcano. First, Wolf volcano lies on the northern periphery of the Galápagos platform; most of the volume of hotspot-related magmatism is to the south, in the central part of the archipelago (the Fernandina–Sierra Negra area; Fig. 1). Second, recent tomographic imaging (Toomey *et al.*, 2001) and seismic study of the mantle Transition Zone (Hooft *et al.*, 2003) indicate that the core of the Galápagos plume lies well to the south of Wolf volcano, just west of Cerro Azul and Fernandina

volcanoes. Third, entrainment does not explain why melting would be deeper and to lower extents at Wolf than at the GSC.

We do not discard the entrainment hypothesis for the Galápagos region, but we consider another mechanism that might explain the dominance of the depleted source in Wolf's magmas: melting at the margins of a thermal and compositional plume that traverses the upper mantle. Several effects may be significant at the margins of an ascending plume. The first is heating of the surrounding ambient mantle by the plume. Jellinek & Manga (2004) showed that the thickness of a thermal boundary layer surrounding a plume that ascends through the mantle is approximately $2{\cdot}3d$, where d is the diameter of the plume. The diameter of the Galápagos plume is unknown, but because the buoyancy flux scales to d^2, the diameter of the Hawaiian plume has been estimated to be 50–75 km (e.g. Griffiths & Campbell, 1991), and the ratio of Hawaii/Galápagos buoyancy fluxes is ~5 (Sleep, 1990), we estimate that the Galápagos plume is 23–35 km in diameter. Consequently, a thermal boundary layer in the ambient mantle roughly 50–80 km wide should surround the Galápagos plume.

In addition, an ascending plume may drag the surrounding mantle up with it in a mechanical boundary layer, causing decompression melting of the ambient mantle where it otherwise would not occur. Continuity of viscous stresses at the interface between the plume and the surrounding mantle demands that

$$\frac{(\eta_{\text{plume}}\nu)}{d} \sim \left(\frac{\eta_{\text{mantle}}\nu}{L}\right)$$

where L is the mechanical boundary layer thickness, η is viscosity, ν is the average velocity of material flowing through the plume conduit, and d is the plume diameter. (A. M. Jellinek, personal communication, 2004). Thus, the width of the mechanical boundary layer surrounding an ascending plume is

$$L \sim (\eta_{\text{mantle}}/\eta_{\text{plume}})d.$$

For a plume diameter of 23–35 km and a viscosity ratio of 100 (appropriate for a temperature difference between the plume and upper mantle of 200°C; Jellinek & Manga, 2004), the mechanical boundary layer surrounding a plume is over 2000 km thick.

Thus, the dominance of depleted mantle magma source characteristics at Wolf volcano is attributable to melting of depleted upper mantle that has been thermally and dynamically affected by the plume, but only lightly contaminated by it. As the plume ascends through the depleted upper mantle, it drags it along and heats it. If, as at the Galápagos hotspot, the lithosphere is sufficiently thin, this depleted upper mantle material is hot enough to reach its solidus by decompression (Fig. 13).

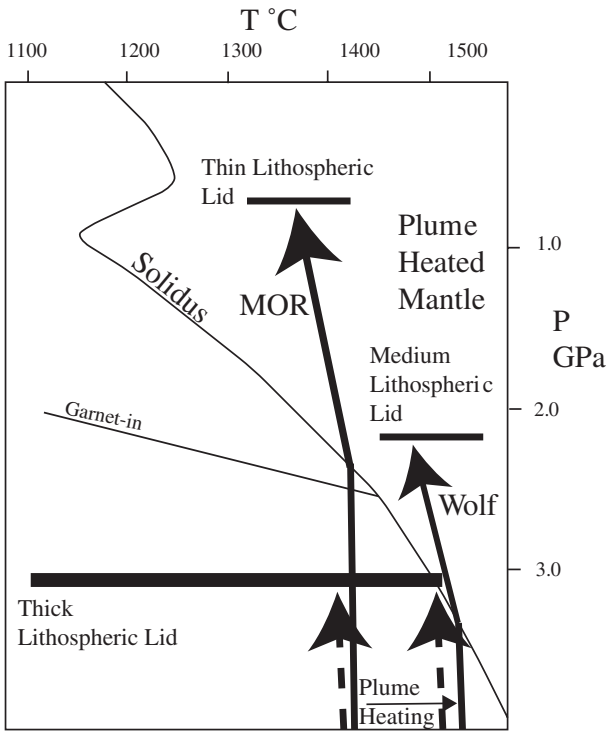

Fig. 13. Schematic model for partial melting at the margins of a mantle plume. Mantle solidus and garnet stability curves are from Asimow *et al.* (2001). Two differences are critical between melting at the GSC and beneath Wolf. First, at deep levels, the ambient mantle is heated by the plume beneath Wolf; this causes the mantle beneath Wolf to intersect the solidus in the presence of garnet. Second, a thicker lithospheric lid at Wolf compared with the GSC prevents mantle upwelling to shallower levels, and the extent of melting is lower. In the mid-plate setting, where the lithosphere is thick enough, melting does not occur in either the ambient mantle or the plume-heated mantle case.

Such a mechanism partly explains the differences in trace and major elements between Wolf and GSC magmas, despite their Nd, Sr, and Pb isotopic similarities. The lithosphere is thicker where it is 10 Myr old at Wolf than it is at the GSC. This thicker lithosphere acts as a lid, preventing the extensive melting that occurs at shallower depths beneath the mid-ocean ridge (e.g. Asimow *et al.*, 2001) and increasing the influence of melts derived at higher pressures (Fig. 13). Similar controls on melting by differences in the thickness of the lithospheric lid near mid-ocean ridges have been proposed for seamounts (e.g. Wilson, 1992) and other ocean islands (e.g. Harpp *et al.*, 2002; Regelous *et al.* 2003).

CONCLUSIONS

Magmas that make up Wolf volcano form when ambient upper mantle is heated and dragged up by the Galápagos plume as it ascends to the west of Fernandina and south of Isabela islands (Toomey *et al.*, 2001; Hooft *et al.*, 2003).

This causes low degrees of melting by decompression of a dominantly depleted upper mantle source. Melts are extracted at greater depths beneath Wolf volcano than those derived beneath the GSC, as indicated by greater geochemical control by garnet.

Ascending magmas cool and react with a cumulate mush and undergo substantial fractionation of olivine + augite + plagioclase before they intrude a subcaldera sill whose top is just below sea level. Further crystallization takes place within the sill, plagioclase accumulates by flotation at its roof, and mafic mush accumulates at its base. Magmas residing within the sill are buffered to a temperature of 1150 ± 11°C.

Magmas erupt through ring dikes that lead to the summit carapace or lateral radial dikes that lead to the subaerial and submarine flanks of the volcano. Although stresses induced by loading of adjacent volcanoes influence the direction of lateral dikes injection, the subaerial rift zones are more diffuse than on Hawaiian shield volcanoes. Once the diffuse rift zones are initiated, they are self-perpetuating, because the topography they build creates stresses that direct later dikes in the same direction. Wolf has undergone at least two stages of caldera collapse, punctuated by a phase of partial refilling of the caldera.

ACKNOWLEDGEMENTS

D.J.G.'s work on Wolf volcano was supported by NSF Grants EAR-9117640 and EAR-0003367, and work on the DRIFT4 cruise by EAR-0002818. WHOI isotope work was funded by EAR-0126097 and OCE-0002461; we thank J. Bluszstajn and J. Curtice for assistance in the laboratory. We acknowledge the logistical support of the Charles Darwin Research Station and permission of the Galápagos National Park Service, without whom this work could not have been accomplished. Antonio Villema got us up the volcano and saved our lives several times. Thanks go to Scottie and Diane for their proficient running of the WSU geoanalytical lab, and Mike Garcia for help with the UH probe. Kaj Hoernle, Jamie Allan, and Pat Castillo provided highly useful and constructive reviews. We thank Ron Frost and Marjorie Wilson for their editorial handling of the manuscript. Mark Jellinek provided help with boundary layers. Peter Mouginis-Mark kindly provided the DEM from TOPSAR data.

REFERENCES

Albarède, F. (1993). Residence time analysis of geochemical fluctuations in volcanic series. *Geochimica et Cosmochimica Acta* **57**, 615–621.

Albarède, F., Luais, B., Fitton, G., Semet, M., Kaminski, E., Upton, G. J., Bachelery, P. & Cheminée, J.-L. (1997). The geochemical regimes of Piton de la Fournaise volcano (Réunion) during the last 530 000 years. *Journal of Petrology* **38**, 171–201.

Allan, J. F. & Simkin, T. (2000). Fernandina Volcano's evolved, well-mixed basalts: mineralogical and petrological constraints on the nature of the Galápagos plume. *Journal of Geophysical Research* **105**, 6017–6031.

Amelung, F., Jonsson, S., Zebker, H. & Segall, P. (2000). Widespread uplift and 'trapdoor' faulting on Galápagos volcanoes observed with radar interferometry. *Nature* **407**, 993–998.

Asimow, P. D., Hirschmann, M. M. & Stolper, E. M. (2001). Calculation of peridotite partial melting from thermodynamic models of minerals and melts; IV, Adiabatic decompression and the composition and mean properties of mid-ocean ridge basalts. *Journal of Petrology* **42**, 963–998.

Bedard, J. H. (1993). Oceanic crust as a reactive filter; synkinematic intrusion, hybridization, and assimilation in an ophiolitic magma chamber, western Newfoundland. *Geology* **21**, 77–80.

Blichert-Toft, J. & White, W. M. (2001). Hf isotope geochemistry of the Galápagos Islands. *Geochemistry, Geophysics, Geosystems* **2**, paper number 2000GC000138.

Chadwick, W. W. & Howard, K. A. (1991). The pattern of circumferential and radial eruptive fissures on the volcanoes of Fernandina and Isabela islands, Galápagos. *Bulletin of Volcanology* **53**, 259–275.

Chadwick, W. W., Jr, De Roy, T. & Carrasco, A. (1991). The September 1988 intracaldera avalanche and eruption at Fernandina volcano, Galápagos Islands. *Bulletin of Volcanology* **53**, 276–286.

Davis, R., Zisk, S., Simpson, M., Edwards, M., Shor, A. & Halter, E. (1993). Hawaii Mapping Research Group bathymetric and side-scan data processing. In: *Oceans '93: Engineering in Harmony With the Ocean: Proceedings, Vol. II.* Piscataway, NJ: IEEE Press, pp. 449–453.

Detrick, R. S., Sinton, J. M., Ito, G., Canales, J. P., Behn, M., Blacic, T., *et al.* (2002). Correlated geophysical, geochemical, and volcanological manifestations of plume–ridge interaction along the Galapagos spreading center. *Geochemistry, Geophysics, Geosystems* **3**(10), 14.

Feighner, M. A. & Richards, M. A. (1994). Lithospheric structures and compensation mechanisms of the Galápagos Archipelago. *Journal of Geophysical Research* **99**, 6711–6729.

Fiske, R. S. & Jackson, E. E. (1972). Orientation and growth of Hawaiian volcanic rifts: the effect of regional structure and gravitational stresses. *Philosophical Transactions of the Royal Society of London, Series A* **329**, 299–326.

Fitton, J. G., Saunders, A. D., Kempton, P. D. & Hardarson, B. S. (2003). Does depleted mantle form an intrinsic part of the Iceland plume? *Geochemistry, Geophysics, Geosystems* **4**, doi:10.1029/2002GC000424.

Fornari, D. J., Kurz, M. D., Geist, D. J., Johnson, P. D., Peckman, U. G. & Scheirer, D. (2001). New perspectives on the structure and morphology of the submarine flanks of Galapagos volcanoes—Fernandina and Isabela. *EOS Transactions, American Geophysical Union, Fall Meeting Supplement* **82**, Abstract T41D-06.

Garcia, M. O., Hulsebosch, T. P. & Rhodes, J. M. (1995). Olivine-rich submarine basalts from the southwest rift zone of Mauna Loa volcano; implications for magmatic processes and geochemical evolution; Mauna Loa revealed; structure, composition, history, and hazards. *Geophysical Monograph, American Geophysical Union* **92**, 219–239.

Geist, D. & Teasdale, R. (2001). Lithospheric evolution of Galápagos magmas. *Transactions of the American Geophysical Union, Fall Meeting Supplement* **82**, Abstract T41D-05.

Geist, D. J., White, W. M. & McBirney, A. R. (1988). Plume asthenosphere mixing beneath the Galápagos Archipelago. *Nature* **333**, 657–660.

Geist, D. J., Howard, K. A., Jellinek, A. M. & Rayder, S. (1994). Volcanic history of Volcán Alcedo, Galápagos Archipelago: a case study of rhyolitic oceanic volcanism. *Bulletin of Volcanology* **56**, 243–260.

Geist, D. J., Naumann, T. R. & Larson, P. L. (1998). Evolution of Galápagos magmas: mantle and crustal fractionation without assimilation. *Journal of Petrology* **39**, 953–971.

Geist, D., White, W., Naumann, T. & Reynolds, R. (1999). Illegitimate magmas of the Galápagos: insights into mantle mixing and magma transport. *Geology* **27**, 1103–1106.

Geist, D., White, W. M., Albarède, F., Harpp, K., Reynolds, R., Blichert-Toft, J. & Kurz, M. D. (2002). Volcanic evolution in the Galápagos: the dissected shield of Volcan Ecuador. *Geochemistry, Geophysics, Geosystems* **3**, 1061, doi:10.1029/2002GC000355.

Geist, D., Naumann, T., Standish, J., Harpp, K., Kurz, M. & Fornari, D. (2003). Diffuse rift zones: subaerial and submarine satellite vents at Wolf Volcano, Galápagos. *EOS Transactions, American Geophysical Union, Fall Meeting Supplement* **84**, Abstract V12G-04.

Ghiorso, M. S. & Sack, R. O. (1995). Chemical mass transfer in magmatic processes IV: a revised and internally consistent thermodynamic model for the interpolation and extrapolation of liquid–solid equilibria in magmatic systems at elevated temperatures and pressures. *Contributions to Mineralogy and Petrology* **119**, 197–212.

Ghiorso, M. S., Hirschmann, M. M., Reiners, P. W. & Kress, V. C., III (2002). The pMELTS: a revision of MELTS for improved calculation of phase relations and major element partitioning related to partial melting of the mantle to 3 GPa. *Geochemistry, Geophysics, Geosystems* **3**, 1030, doi:10.1029/2001GC000217.

Graham, D. W., Christie, D. M., Harpp, K. S. & Lupton, J. E. (1993). Mantle plume helium in submarine basalts from the Galápagos platform. *Science* **262**, 2023–2026.

Gregg, T. K. P. & Fink, J. H. (1995). Quantification of submarine lava-flow morphology through analog experiments. *Geology* **23**, 73–76.

Griffiths, R. W. & Campbell, I. H. (1991). On the dynamics of long-lived plume conduits in the convecting mantle. *Earth and Planetary Science Letters* **103**, 214–227.

Gripp, A. E. & Gordon, R. G. (1990). Current plate velocities relative to the hotspots incorporating the NUVEL-1 global plate motion model. *Geophysical Research Letters* **17**, 1109–1112.

Grove, T. L., Kinzler, R. J. & Bryan, W. B. (1992). Fractionation of mid-ocean ridge basalt (MORB). In: Morgan, J. P., Blackman, D. K. & Sinton, J. M. (eds) *Mantle Flow and Melt Generation at Mid-Ocean Ridges. Geophysical Monograph, American Geophysical Union* **71**, 281–310.

Hanan, B. B., Blichert-Toft, J., Kingsley, R. & Schilling, J.-G. (2000). Depleted Iceland mantle plume geochemical signature; artifact of multicomponent mixing? *Geochemistry, Geophysics, Geosystems* **1**, paper number 1999GC000009.

Hardarson, B. S. & Fitton, J. G. (1997). Mechanisms of crustal accretion in iceland. *Geology* **25**, 1043–1046.

Harpp, K. S. & White, W. M. (2001). Tracing a mantle plume; isotopic and trace element variations of Galápagos seamounts. *Geochemistry, Geophysics, Geosystems* **2**, paper number 2000GC000137.

Harpp, K. S., Wirth, K. R. & Korich, D. J. (2002). Northern Galápagos Province; hotspot-induced, near-ridge volcanism at Genovesa Island. *Geology* **30**, 399–402.

Harpp, K. S., Fornari, D. J., Geist, D. J. & Kurz, M. D. (2003). Genovesa Submarine Ridge: a manifestation of plume–ridge interaction in the northern Galápagos Islands. *Geochemistry, Geophysics, Geosystems* **4**, doi:10.1029/2003GC000531.

Hirschmann, M. M. & Stolper, E. M. (1996). A possible role for garnet pyroxenite in the origin of the 'garnet signature' in MORB. *Contributions to Mineralogy and Petrology* **124**, 185–208.

Hoernle, K., Werner, R., Morgan, J. P., Garbe-Schoenberg, D., Bryce, J. & Mrazek, J. (2000). Existence of complex spatial zonation in the Galápagos Plume for at least 14 m.y. *Geology* **28**, 435–438.

Hooft, E. E., Toomey, D. R. & Solomon, S. C. (2003). Anomalously thin transition zone beneath the Galápagos hotspot. *Earth and Planetary Science Letters* **216**, 55–64.

Jellinek, A. M. & Manga, M. (2004). Links between long-lived hot spots, mantle plumes, d", and plate tectonics. *Reviews of Geophysics* **42**, paper number 2003RG000144.

Johnson, D. M., Hooper, P. R. & Conrey, R. M. (1999). XRF analysis of rocks and minerals for major and trace elements on a single low dilution Li-tetraborate fused bead. *Advances in X-ray Analysis* **41**, 843–867.

Kurz, M. D. (1986). *In-situ* production of cosmogenic terrestrial helium and some applications to geochronology. *Geochimica et Cosmochimica Acta* **50**, 2855–2862.

Kurz, M. D. & Geist, D. (1999). Dynamics of the Galápagos hotspot from helium isotope geochemistry. *Geochimica et Cosmochimica Acta* **63**, 4139–4156.

Kurz, M. D. & Jenkins, W. J. (1981). The distribution of helium in oceanic basaltic glasses. *Earth and Planetary Science Letters* **53**, 41–54.

Kurz, M., Fornari, D., Geist, D. & Shipboard Scientific Party (2001). Cruise Report DRIFT Leg-4 R/V *Roger Revelle* August 23 to September 24, 2001. http://science.whoi.edu/galap_rv_drft4/index.html

Lange, R. L. & Carmichael, I. S. E. (1990). Thermodynamic properties of silicate liquids with emphasis on density, thermal expansion and compressibility. In: Nicholls, J. & Russell, J. K. (eds) *Modern Methods of Igneous Petrology; Understanding Magmatic Processes. Mineralogical Society of America, Reviews in Mineralogy*, **24**, 25–64.

Marsh, B. D. (1981). On the crystallinity, probability of occurrence, and rheology of lava and magma. *Contributions to Mineralogy and Petrology* **78**, 85–98.

McBirney, A. R. & Williams, H. (1969). *Geology and Petrology of the Galápagos Islands. Geological Society of America, Memoirs* **118**, 197 pp.

McKenzie, D. & O'Nions, R. K. (1991). Partial melt distributions from inversion of rare earth element concentrations. *Journal of Petrology* **32**, 1021–1091.

Morgan, W. J. (1971). Convection plumes in the lower mantle. *Nature* **230**, 42–43.

Mouginis-Mark, P. J., Rowland, S. K. & Garbeil, H. (1996). Slopes of western Galápagos volcanoes from airborne interferometric radar. *Geophysical Research Letters* **23**, 3767–3770.

Naumann, T. & Geist, D. (2000). Physical volcanology and structural development of Cerro Azul volcano, Isabela island, Galápagos: implications for the development of Galápagos-type shield volcanoes. *Bulletin of Volcanology* **61**, 497–514.

Naumann, T. R., Geist, D. & Kurz, M. D. (2002). Petrology and geochemistry of Volcan Cerro Azul: petrologic diversity among the western Galápagos volcanoes. *Journal of Petrology* **43**, 859–883.

Naumann, T. R., Gibler-Moore, K. & Nelson, L. K. (2003). Geology of Volcán Darwin, Isabela Island, Galápagos Archipelago. *Geological Society of America, Abstracts with Programs* **35**, 324.

Pearce, T. H. & Kolisnik, A. M. (1990). Observations of plagioclase zoning using interference imaging. *Earth-Science Reviews* **29**, 9–26.

Regelous, M., Hofmann, A. W., Abouchami, W. & Galer, S. J. G. (2003). Geochemistry of lavas from the Emperor Seamounts, and the geochemical evolution of Hawaiian magmatism from 85 to 42 Ma. *Journal of Petrology* **44**, 113–140.

Reynolds, R. W. & Geist, D. J. (1995). Petrology of lavas from Sierra Negra volcano, Isabela Island, Galápagos Archipelago. *Journal of Geophysical Research* **100**, 24537–24553.

Reynolds, R., Geist, D. & Kurz, M. (1995). Physical volcanology and structural development of Sierra Negra volcano, Galápagos Archipelago. *Geological Society of America Bulletin* **107**, 1398–1410.

Rongstadt, M. (1992). HAWAII MR-1: a new underwater mapping tool. Paper presented at International Conference on Signal Processing and Technology, Institute of Electrical and Electronic Engineers, San Diego, CA.

Rowland, S. K. & Garbeil, H. (2000). Slopes of oceanic basalt volcano. In: Mouginis-Mark, P. J., Crisp, J. A. & Fink, J. H. (eds) *Remote Sensing of Active Volcanism. Geophysical Monograph, American Geophysical Union* **116**, 223–247.

Rowland, S. K. & Munro, D. C. (1992). The caldera of Volcan Fernandina: a remote sensing study of its structure and recent activity. *Bulletin of Volcanology* **55**, 97–109.

Rowland, S. K. & Walker, G. P. L. (1990). Pahoehoe and aa in Hawaii: volumetric flow rate controls the lava structure. *Journal of Volcanology and Geothermal Research* **52**, 615–628.

Ryland, S. L. (1971). A gravity and magnetic study of the Galápagos Islands. M.S. thesis, University of Missouri, Columbia, p. 57.

Schilling, J. G., Kingsley, R. H. & Devine, J. D. (1982). Galapagos hot spot–spreading center system; 1, spatial petrological and geochemical variations (83W–101W). *Journal of Geophysical Research* **87**, 5593–5610.

Schilling, J.-G., Fontignie, D., Blichert-Toft, J., Kingsley, R. & Tomza, U. (2003). Pb–Hf–Nd–Sr isotope variations along the Galápagos Spreading Center (101–83°W): constraints on the dispersal of the Galápagos mantle plume. *Geochemistry, Geophysics, Geosystem* **4**, 8512, doi:10.1029/2002GC000495.

Simkin, T. (1972). Origin of some flat topped volcanoes and guyots. *Geological Society of America, Memoirs* **132**, 183–193.

Simkin, T. & Siebert, L. (1994). *Volcanoes of the World*, 2nd edn. Tucson, AZ: Geoscience Press, 349 pp.

Sinton, C. S., Christie, D. M. & Duncan, R. A. (1996). Geochronology of Galápagos seamounts. *Journal of Geophysical Research* **101**, 13689–13700.

Sinton, J. M. & Detrick, R. (1992). Mid-ocean ridge magma chambers. *Journal of Geophysical Research* **97**, 197–216.

Sleep, N. H. (1990). Hotspots and mantle plumes; some phenomenology. *Journal of Geophysical Research* **95**, 6715–6736.

Standish, J., Geist, D., Harpp, K. & Kurz, M. (1998). The emergence of a Galápagos shield volcano, Roca Redonda. *Contributions to Mineralogy and Petrology* **133**, 136–148.

Toomey, D. R., Hooft, E. E., Solomon, S. C., James, D. E. & Hall, M. L. (2001). Upper mantle structure beneath the Galápagos archipelago from body wave data. *Transactions of the American Geophysical Union, Fall Meeting Supplement* **82**, Abstract T41D-04.

Walker, G. P. L. (1988). Three Hawaiian calderas; an origin through loading by shallow intrusions? *Journal of Geophysical Research* **93**, 14773–14784.

White, W. M. & Hofmann, A. W. (1978). Geochemistry of the Galápagos Islands: implications for mantle dynamics and evolution. *Carnegie Institution of Washington Yearbook* **77**, 596–606.

White, W. M., McBirney, A. R. & Duncan, R. A. (1993). Petrology and geochemistry of the Galápagos Islands: portrait of a pathological mantle plume. *Journal of Geophysical Research* **98**, 19533–19564.

Williams, H. & McBirney, A. R. (1979). *Volcanology*. San Francisco, CA: Freeman Cooper, p. 397.

Wilson, D. S. (1992). Focused mantle upwelling beneath mid-ocean ridges; evidence from seamount formation and isostatic compensation of topography. *Earth and Planetary Science Letters* **113**, 41–55.

Wilson, D. S. & Hey, R. N. (1995). History of rift propagation and magnetization intensity for the Cocos–Nazca spreading center. *Journal of Geophysical Research* **100**, 10041–10056.